Integrated Adsorptive and Photocatalytic Treatment of Levofloxacin and Cadmium from Wastewater using Biomass derived Carbon-ZnO Composite

Master of Philosophy

in

Environmental Sciences

By

SABA GUL

Registration No. 02312111014

DEPARTMENT OF ENVIRONMENTAL SCIENCES

FACULTY OF BIOLOGICAL SCIENCES

QUAID-I-AZAM UNIVERSITY

ISLAMABAD, PAKISTAN

2023

Integrated Adsorptive and Photocatalytic Treatment of Levofloxacin and Cadmium from Wastewater using Biomass derived Carbon-ZnO Composite

Master of Philosophy

in

Environmental Sciences

By

SABA GUL

Registration No. 02312111014

DEPARTMENT OF ENVIRONMENTAL SCIENCES

FACULTY OF BIOLOGICAL SCIENCES

QUAID-I-AZAM UNIVERSITY

ISLAMABAD, PAKISTAN

2023

DEDICATION

I dedicate this thesis to my beloved Parents and my sister who have offered their affection and support during my studies; especially my mother for always believing in me, praying for me and giving me courage.

AUTHOR'S DECLARATION

I, **"Saba Gul"** (Registration No. 02312111014) hereby declare that my M.Phil. thesis titled as **"Integrated Adsorptive and Photocatalytic Treatment of Levofloxacin and Cadmium from Wastewater using Biomass derived Carbon-ZnO Composite"** is all my own effort done in Renewable Energy Advancement Lab, Department of Environmental Sciences Quaid-i-Azam University, Islamabad. All the investigations, findings, results, conclusions of this research have neither been previously presented anywhere nor published in any local or international forum.

Saba Gul

PLAGIARISM UNDERTAKING

I, **Saba Gul**, hereby state that my M.Phil. Thesis titled as **"Integrated Adsorptive and Photocatalytic Treatment of Levofloxacin and Cadmium from Wastewater using Biomass derived Carbon-ZnO Composite"** is solely my research work with no significant contribution from any other person. Small contribution/help whatever taken has been duly acknowledged and that complete thesis has been written by me.

I understand zero tolerance policy of the HEC and Quaid-i-Azam University, Islamabad, towards plagiarism. Therefore, I as an author of the above titled thesis declare that no portion of my thesis has been plagiarized and any material used as reference is properly referred/cited.

I undertake that if I am found guilty of any form of plagiarism in the above titled thesis even after the award of M.Phil. degree, the university reserves the right to withdraw/revoke my M.Phil. degree and that HEC and the university has the right to publish my name on the HEC/University website on which the names of students are placed who submitted plagiarism.

Saba Gul

TABLE OF CONTENTS

ACKNOWLEDGEMENT

I am very thankful to **Allah Almighty**, who is the most merciful and beneficent, who has blessed me with all His blessings and has given me the strength to finish my work in time.

I am fortunate to be under the supervision of **Dr. Abdullah Khan** who has provided me all the guidance and support that was needed to complete this task.

I am highly indebted to my Parents, family and friends especially **Aqsa Huma**, **Anila Ayub, Abdul Saboor** and **Asad Ali** who helped me out with their experiences and moral support.

I could not have finished this document without the support from my lab fellows specially **Subul Huda**, **Fariah Salam**, **Imran Rameel** and **Mehar Wali**. Thank you all, for being so cooperative and supportive whenever I needed your help and guidance. I wish you people the best.

Saba Gul

LIST OF ABBREVIATIONS

ECs	Emerging Contaminants
LEV	Levofloxacin
UV-Vis	Ultraviolet Visible Spectroscopy
XRD	X-Ray Diffraction
APIs	Active Pharmaceutical Ingredients
AOPs	Advance Oxidation Processes
WWTP	Wastewater Treatment Plant
CB	Conduction Band
VB	Valance Band
eV	Electron Volt
SEM	Scanning Electron Microscopy
FTIR	Fourier-Transform Infrared Spectroscopy
EDS	Energy Dispersive X-Ray Spectroscopy
ppm	Parts per million
Eg	Bandgap Energy
EDTA	Ethylene Diamine Tetra Acetic Acid

LIST OF FIGURES

LIST OF TABLES

HIGHLIGHTS

- A novel ZnO and carbon based composite was synthesized for the adsorptive and photocatalytic treatment of emerging contaminants like levofloxacin and cadmium.
- The C-ZnO composite exhibit better adsorption compared to photoredox behviour.
- The enhanced activity of the coupled composite materials could be used as a template for application specific design of materials.

GRAPHICAL ABSTRACT

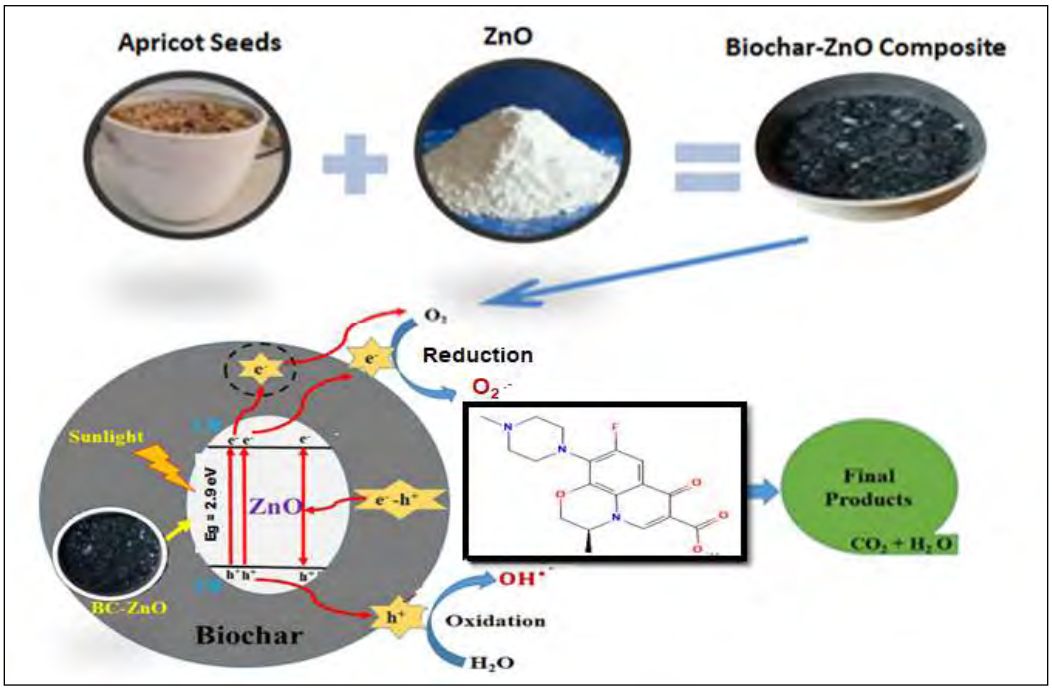

ABSTRACT

ZnO has been combined with several carbonaceous substrates, such as graphene and carbon nanotubes, to enhance its photocatalytic performance of carbon-based ZnO photocatalysts. In the quest for sustainability biomass derived carbon supports low-cost alternatives to traditional synthetic routes. In this study, a biomass derived carbon made from apricot seeds was used to synthesize C-ZnO composite with a aim to address many intrinsic ZnO issues such as (charge recombination, wider band gap, and poor visible light absorption) in a photocatalytic process. In comparison to pure ZnO, the prepared composite had a lower band gap (2.93 eV) and extended visible light absorption regime. Subsequently it was employed to degrade Levofloxacin and reduce Cadmium. The material showed enhanced adsorptive-photocatalytic degradation efficiency attaining a 68% degradation for levofloxacin and 56% photoreduction for cadmium. The microstructural assessment of the material showed that carbon-ZnO composite is a stable, economical and sustainable option for the cleaning wastewater.

Keywords: composite, low-cost, apricot, bandgap, cadmium, levofloxacin, adsorption, photocatalysis, wastewater.

1. INTRODUCTION

1.1 Water Scarcity and Contamination

Water plays a vital role in our lives. Maintaining access and availability to safe drinking water is a pressing sustainability challenge. The world consumption of water has almost doubled within a few decades. Water scarcity is plaguing nations due to number of factors like rapid increase in population growth, urbanization and climate change. Being intensively used for agricultural purposes, in industries, at home, transportation and combined with issues of climate change, water is becoming a scarce resource. [1]

There are significant global issues with environmental contamination and a lack of natural renewable energy sources. The rapid urbanization, industrialization, and population growth of the world speed up the use of non-renewable energy and increase pollution in the air and waterways. Discharges of wastewater that have been mistreated have a negative impact on the ecology and the general public's health. Therefore, we must come up with a practical, affordable, and long-lasting solution to this adverse situation.

1.2 Pharmaceuticals as Emerging Contaminants

Organic contaminants, sometimes referred to as emerging contaminants (ECs), are capturing the attention of the public due to their severe degradation of water quality and the difficulties they present to conventional water treatment systems in effectively removing them. Owing to the advances in science and technology, ECs have been contaminating the environment ever since 19th century, but they were only recently recognised as major dangerous water pollutants. Any natural or manmade chemical or microorganism, if not properly controlled, may have harmful effects on the environment or on human health. ECs are made up of extremely polar, acidic/alkaline substances like

surfactants, hormones, pesticides, dioxins, and pharmaceuticals and personal care items. [3]

Pharmaceuticals are one of the most significant environmental concerns despite the fact that their ambient concentrations are low due to their constant input and persistence into the aquatic ecosystem. The use of pharmaceuticals is rising globally, especially in quickly expanding nations, due to rising living standards and drug affordability. It is undoubtedly incorrect to assume that pharmaceutical output and use will remain roughly constant. The possibility exists that medications, their metabolites, and transformation products could penetrate the aquatic environment and eventually make their way into drinking water supplies if they are not removed during sewage treatment or sorbed in soil. (**Figure 1.1**) [4]

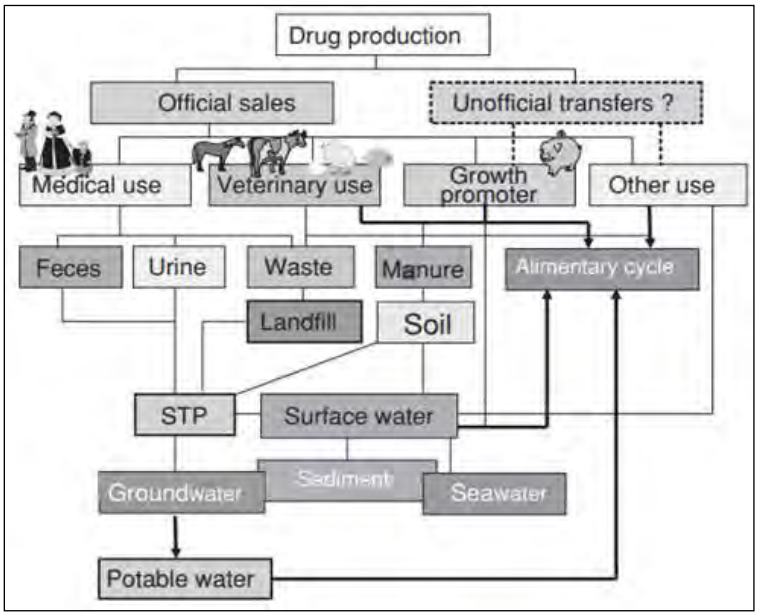

Figure 1.1 pathways of input and distribution of pharmaceuticals in the environment. STP, sewage treatment plant

1.2.1 Active Pharmaceutical Ingredients (APIs)

Pharmaceuticals are made up of excipients, additives, and one or more active pharmaceutical ingredients (APIs). They are often of minor importance for the environment. From a chemical point of view, APIs include a broad spectrum of so-called

small molecules with various physicochemical and biological properties (their molecular weights typically fall between 200 and 500 Da). An API's environmental fate may be greatly impacted by even minor modifications to its chemical structure [5].

1.3 Heavy Metal Pollution

In general, metals and metalloids with densities greater than 5 g/cm3 are referred to be heavy metals. Due to comparable chemical characteristics and environmental behavior, metalloids like arsenic (As) frequently fall under the heavy metal umbrella. Heavy metal pollution is undetectable, ongoing, and permanent. This type of pollution threatens the health of animals and humans by way of the food chain in addition to damaging the atmosphere, water bodies, and crops.[6] **(Figure 1.2)**.[7]

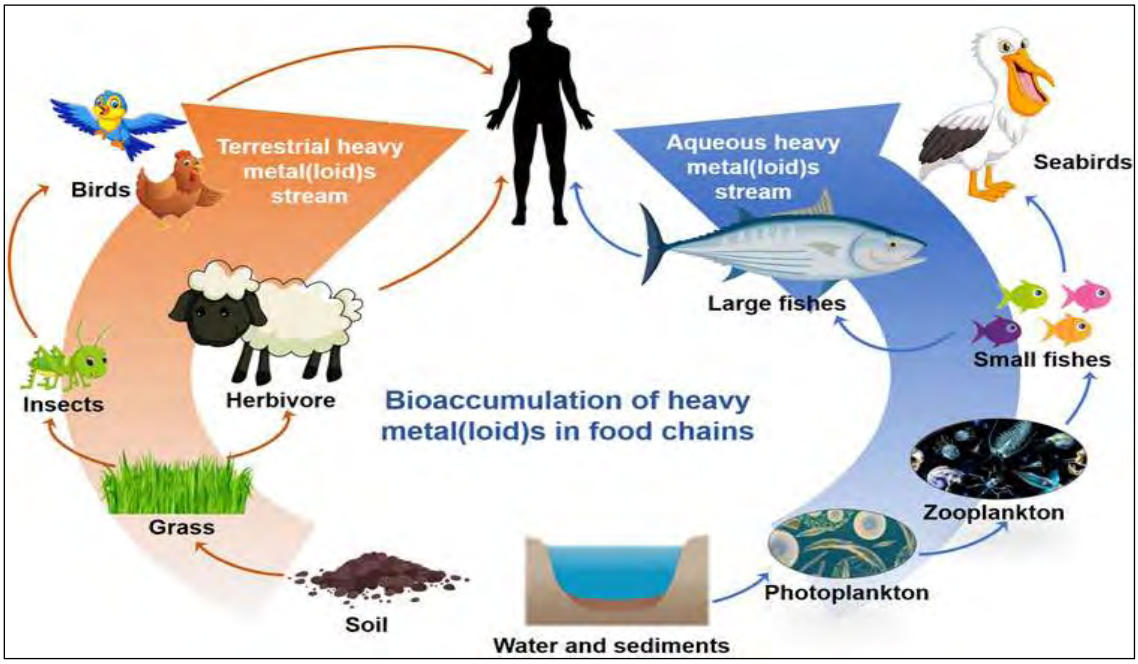

Figure 1.2 a schematic model of bioaccumulation of HMs in terrestrial and aqueous food chains

Due to the mobility and toxicity of these contaminants in natural water ecosystems, heavy metal pollution of wastewater is currently the biggest environmental issue endangering human life worldwide. The fact that the heavy metal ions cannot be broken down and eliminated makes them stable environmental pollutants. [8]

1.3.1 Source of Contamination of heavy metals in Water

Natural Sources: Volcanic eruptions, metal-containing rock weathering, sea-salt sprays, and forest fires are a few examples of geological/natural sources.

Anthropogenic Sources: Human activities such as mining, smelting, burning fossil fuels, disposing of trash, corrosion, and agricultural practices are examples of anthropogenic causes of heavy metal contamination. [9]

Some of the types of heavy metals and their toxic effect on human health are enumerated in **Table 1.1**.

Table 1.1 types of heavy metals and their toxic effect on human health

Lead	Cadmium	Mercury	Arsenic
Memory and Concentration Problems	Renal Failure	Spontaneous Abortion in Women	Coagulates Protein
High Blood Pressure	Hyperactivity	Carcinogenic Effect	Muscle Weakness
Carcinogenic Effect	Softening of Bones	Gastrointestinal Disorders	Nerve Inflammation
Reproductive Problems	Carcinogenic Effect	Gingivitis and Stomatitis	Neurotoxic Effect

1.4 Pollutants of Interest

1.4.1 Cadmium

Figure 1.3 cadmium (Cd)

Cadmium is an element with soft, silvery white color, lustrous, and electropositive properties. It has no taste or smell and is extremely lethal [10]. Majority of the cadmium used is a byproduct of the manufacture of metals like zinc, lead, and copper. Cadmium can be

generated in a variety of commercial ways. In addition, it can be found in batteries, fertilizers, cigarettes, metal coatings and also in bright red, yellow and orange pigments seen in certain glass or ceramic paint. [11]

1.4.1.1 Cadmium Sources and its Toxicity

Volcanic eruptions and weathering processes naturally release cadmium into the atmosphere, where it eventually precipitates into bodies of water. House dust can expose people to cadmium in places with toxic soils. Air cadmium values in unpopulated and unpolluted places are less than 1 ng/m^3.

Plant-based foods typically have greater Cd concentrations than dairy items rice and wheat for instance. Compared to omnivores, vegetarians and shellfish consumers may intake more cadmium. Consuming rice is one of the main ways that humans are exposed to cadmium.[12]

1.4.2 Levofloxacin

Figure 1.4 levofloxacin (LEV)

Due to its widespread action, bacterial disinfection, and good oral-intake qualities, the fluoroquinolone antibiotic levofloxacin (LEV) has been utilised in both human and veterinary medicine throughout the world.[13]

LEV is being used extensively in humans, animals, aquaculture, and agriculture due to its ability to treat a number of serious bacterial diseases. Through the food chain, residual levels of the antibiotic are released into the environment. Long-term contact with LEV causes the harmful evolution of low-level antibacterial resistance, which raises the chance of "superbug" development, a condition that results from successive multiple mutations.

Some common antibiotics including levofloxacin are given in **Table 1.2** along with their concentration in Pakistan both in surface and wastewater.

Table 1.2 antibiotic concentration in Pakistan both in surface and wastewater

Antibiotics	Surface water ng/L	Wastewater ng/L
Levofloxacin	19.2	447
Clarithromycin	19.8	100.2
Azithromycin	2.63	14.91
Erythromycin	36.2	364.2
Sulfamethoxazole	325.8	7745

1.4.2.1 Fate of Levofloxacin in the Environment

There are three elements that could have an impact on how pharmaceutical waste behaves in the environment; it may ultimately mineralize to carbon dioxide and water, it may be retained in the sludge because is lipophilic and not readily degradable or in case it is biologically active, it may metabolise into a more durable hydrophilic component, pass through the WWTP, then discharge into water bodies where it may affect the organisms.

The majority of these chemicals are adsorbed on sludge from WWTPs because of their strong affinity for soil and consumption. Levofloxacin may be transmitted to plants by the usual practise of utilising this sludge as fertiliser, entering the human food chain. Because of this, it's essential to devise treatments that can effectively eliminate or neutralise these hazardous substances [14].

1.5 Wastewater Treatment Methods

There are several treatment procedures that combine physical, chemical, and biological treatments. Each treatment method has advantages and disadvantages that vary depending on its efficiency, generation of sludge, and toxic byproducts. These factors are in addition to capital and operating costs [15].

1.5.1 Biological methods

In biological wastewater treatment methods various microbes and enzymes are used to remove different kinds of toxicity from water.

1.5.2 Chemical methods

Using different types of chemicals to clean wastewater for the purpose of drinking, following well known methods are observed; ozonation, chlorination, precipitation and chemical oxidation.

1.5.3 Traditional physical methods

Adsorption, ultrafiltration and reverse osmosis are some of the traditional physical methods.

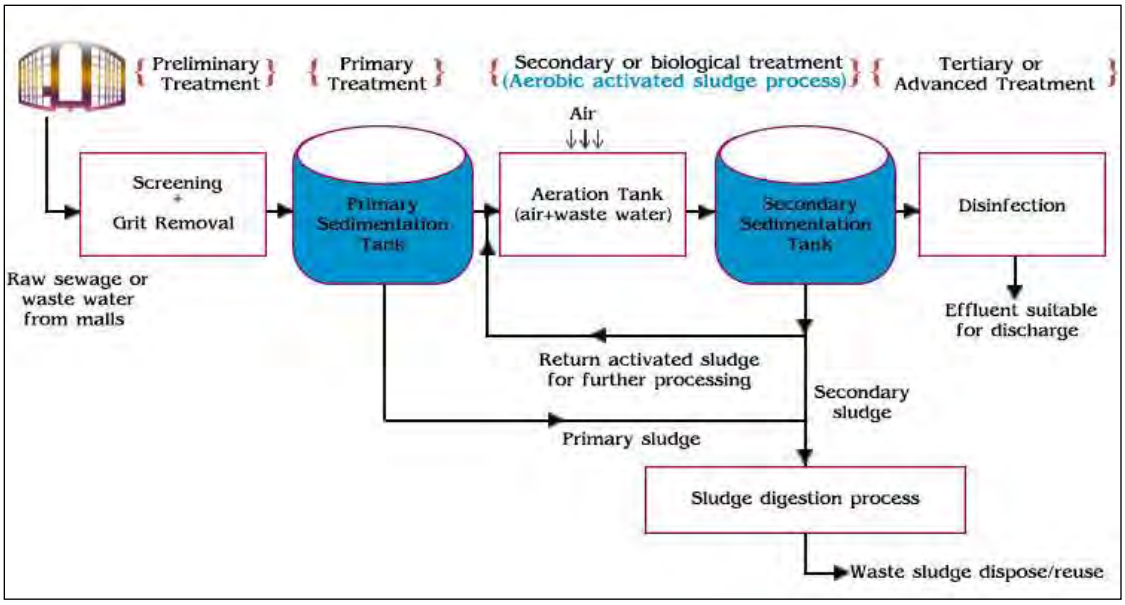

Figure 1.5 an overview of wastewater treatment system

1.6 Adsorption and Photocatalysis; a way forward

There are numerous technologies available today for treating pollutants, including adsorption, membrane separation, biodegradation, electrochemical degradation, chemical precipitation, and photocatalysis. With regard to these, photocatalysis can breakdown organics and oxidize them into a variety of safe and harmless inorganic compounds, such

as CO_2 and H_2O, while the adsorption approach has a wide range of applications due to its straightforward operation, low cost, and high efficiency.

1.6.1 Adsorption mechanism

Adsorption is the chemical or physical interaction that causes atoms, ions, or molecules to stick to the surface of a substrate. Adsorption is a very promising technique in terms of its capacity to be sustained over time, ease of use, and economic viability.

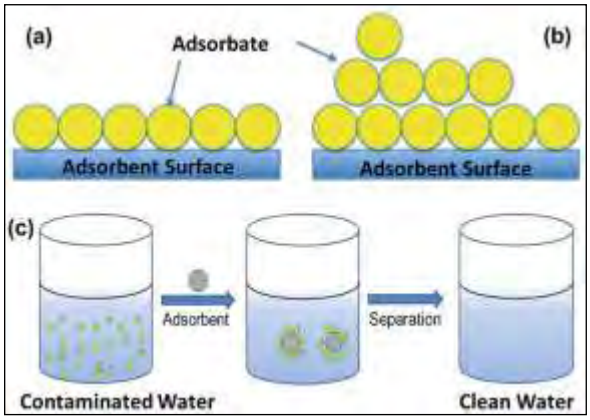

Figure 1.6 mechanism of adsorption

Adsorbate migration typically takes place in this process in three steps beginning with the migration of the adsorbate to the adsorbent's border shell followed by intraparticle diffusion into pores and solute adsorption and desorption [16].

1.6.2 Principle of Photocatalysis

When light falls on the surface of semiconductor electrons are excited and jumped on the conduction band creation a hole on the valence band**. (Figure 1.7)**

$$\text{Semiconductor} + \text{Light} \rightarrow e^- + h^+ \qquad \textbf{(1.1)}$$

Now these two bodies get into a redox reaction where other species are already present on catalyst surface. Hole h^+ can react with H_2O molecule which is bound to surface and produce $OH^{\cdot}$ and on other side e^- can react with O_2 and reduce to superoxide radical anion of oxygen $O_2^{-\cdot}$.

$$H_2O + h^+ \rightarrow OH^{\cdot} + H^+ \qquad \textbf{(1.2)}$$

$$O_2 + e^- \rightarrow O_2^{-\cdot} \qquad \textbf{(1.3)}$$

The hydroxide radicals and oxygen radical anion thus formed can react with organic and inorganic pollutants (R).[17]

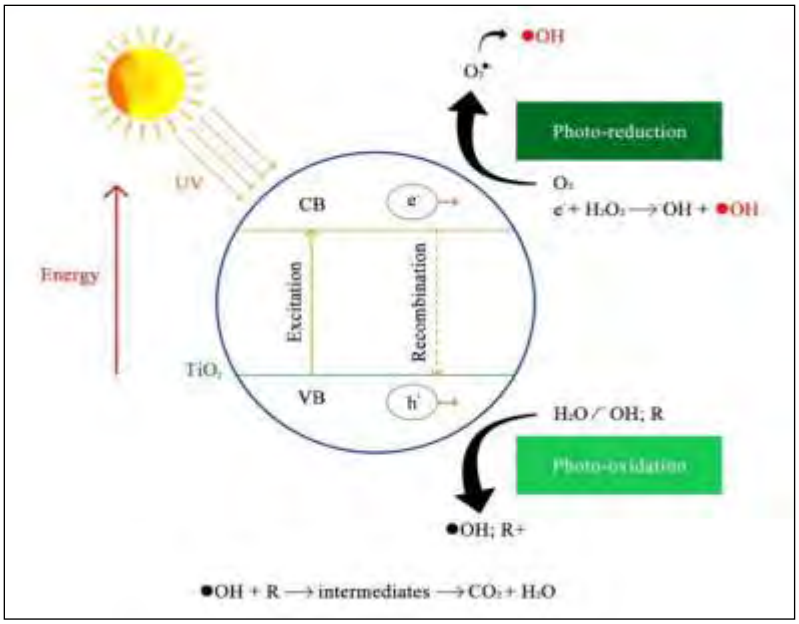

Figure 1.7 mechanism of photocatalysis

The adsorptive and catalytic reactions depend heavily on adsorbents and catalysts. Traditional adsorbents have restricted applications due to their weak regeneration capabilities, low adsorption capacities, and small specific surface areas. Therefore, in order to increase adsorption and photocatalytic performance, novel material alternatives must be developed.

1.6.3 Biochar-supported Photocatalysts

Incorporating secondary materials for enhancing the properties of the photocatalysts, has received increasing attention in recent years. Significant attention is being paid to biochar as a supportive substance for catalytic nanoparticles in this regard.

Using pyrolysis, hydrolysis, gasification, and carbonization techniques, waste biomass is converted into biochar, a low-cost, stable, sustainable substance. In comparison to the bare semiconductor photocatalyst, the produced composite has superior surface characteristics and better photocatalytic competency [18].

1.6.4 Biomass derived Carbon and ZnO Composite

Recently, it has been demonstrated that TiO_2 and ZnO, due to their benign nature, abundance, affordability, high stability, and potent UV light absorption, are efficient heterogeneous photocatalysts for the degradation of different contaminants. ZnO is considered to be a better photocatalyst than TiO_2 due to its low cost, strong excitation binding energy (60 meV), and high UV light absorbance efficiency.

However, there are also drawbacks to employing ZnO for wastewater treatment, such as its greater bandgap (3.37 eV), low ability to absorb visible light, and rapid electron-hole pair recombination, all of which render ZnO ineffective.[19].

Figure 1.8 C - ZnO composite

In order to overcome ZnO's limitations, carbonaceous substrates including graphene, CNTs, and biochar have been utilised to embed ZnO with in order to create ZnO-based photocatalysts. Due to its distinct surface characteristics, easily modifiable functional groups, chemical stability, and electrical conductivity, biochar makes a good platform for a variety of catalytic nanoparticles.

The high specific surface of biochar, along with the dispersion of ZnO nanoparticles over its surface, can be used to obtain more reactive sites, increasing the photodegradation capacity of the composite catalyst.[20]

1.7 Problem Statement

The production and application of heavy metals and pharmaceutical products have significantly increased, leading to a rise in environmental pollution. Even at low concentrations, these chemicals can have detrimental health effects on both humans and animals. They persist in the ecosystem, causing contamination in aquatic environments. Conventional methods have proven ineffective in completely removing these contaminants from water. One potential solution is photocatalysis using biochar-

supported photocatalysts. Additionally, the use of low-cost adsorbents in an adsorption process is a promising alternative to mitigate these issues.

1.8 Objectives

In this context, following study objectives were considered:

- Synthesize composite photocatalyst by impregnating ZnO nanoparticles on a biomass derived carbon synthesized from the pyrolysis of Apricot seeds
- Study adsorptive and photocatalytic measurements of Levofloxacin and Cadmium from wastewater
- Evaluate the effects of pollutant concentration, pH and catalyst dose on the degradation of both pollutants
- Compare and quantify the efficiency of the synthesized catalyst.

2. MATERIALS AND METHODS

2.1 Materials and Reagents

The seeds of Apricot, a commonly found fruit in or country, were collected from the local market. Levofloxacin (LEV), the precursor of Cadmium Acetate dihydrate ($Cd(CH_3COO)2.2H_2O$, 99% pure), Hydrochloric acid (HCl, 98%), Zinc Acetate dihydrate ($Zn(CH_3COO)2.2H_2O$, 99% pure) and Sodium hydroxide (NaOH, 99%) all were obtained from Sigma Aldrich. Deionized water was used to prepare required solution.

2.2 Pretreatment of Biomass

Prior to using distilled water, the apricot seeds were rinsed with tap water to remove contaminants. After being cleaned, the seeds were dried in the sun. The seeds were pounded into a fine powder biomass using a pestle and mortar after they had totally dried. After that, a sieve shaker was used to separate the harvested apricot seed biomass into particles as fine as 150 µm. Prior to use in the experiment, it was sieved and then kept in an airtight tube.

2.3 Preparation of Biochar

Using pyrolysis, apricot seed powder was added to a crucible to create charcoal. At a heating rate of $10 \pm 1\ ^{o}C\ min^{-1}$ and a temperature of $520 \pm 10\ ^{o}C$ for 4 hours, the crucible was kept in the muffle furnace for pyrolysis.

The intrinsic properties of biochar are significantly influenced by the temperature of the pyrolysis process. Following pyrolysis, the produced biochar was allowed to cool at room temperature **(Figure 2.1).** To achieve a pH of 7, the produced biochar material was washed with HCl solution and distilled water. After that, the biochar's moisture content was reduced by heating in an oven at $90 \pm 1\ ^{o}C$.

Figure 2.1 synthesized biochar after pyrolysis

2.4 Preparation of Pure ZnO Nanoparticles

It was carried out using the wet precipitation approach. pure ZnO photocatalyst nanoparticles were created. In a nutshell, $Zn(CH_3COO)_2.2H_2O$ solution was added to a beaker along with NaOH solution. A magnetic stirrer was used to continually mix the NaOH and Zn $(CH_3COO)_2.2H_2O$ combination before it was sonicated (for an hour) to create a homogenous mixture. The solution was centrifuged at 8000 rpm to separate the solid white precipitates, which were then dried overnight at 80 ± 1 ^oC in an oven. The white precipitates were then heated to 400°C for 4 hours in a muffle furnace designed to calcine solid particles in order to produce ZnO- nanoparticles.

2.5 Preparation of the Composite

The in-situ wet precipitation approach was used to create the Carbon-ZnO composite. In detail, 100 ml of 0.1 M zinc acetate solution was added dropwise once 1000 mg of BC was added to 50 ml of 0.05 M NaOH, all while being continuously stirred. The mixture was sonicated to create a homogeneous mixture followed by centrifugation at 8000 rpm for 5 minutes which removed the moisture before drying the resulting white-greyish

precipitates overnight at 85 ± 10 °C. The schematic representation of C-ZnO synthesis is given in **Figure 2.2**.

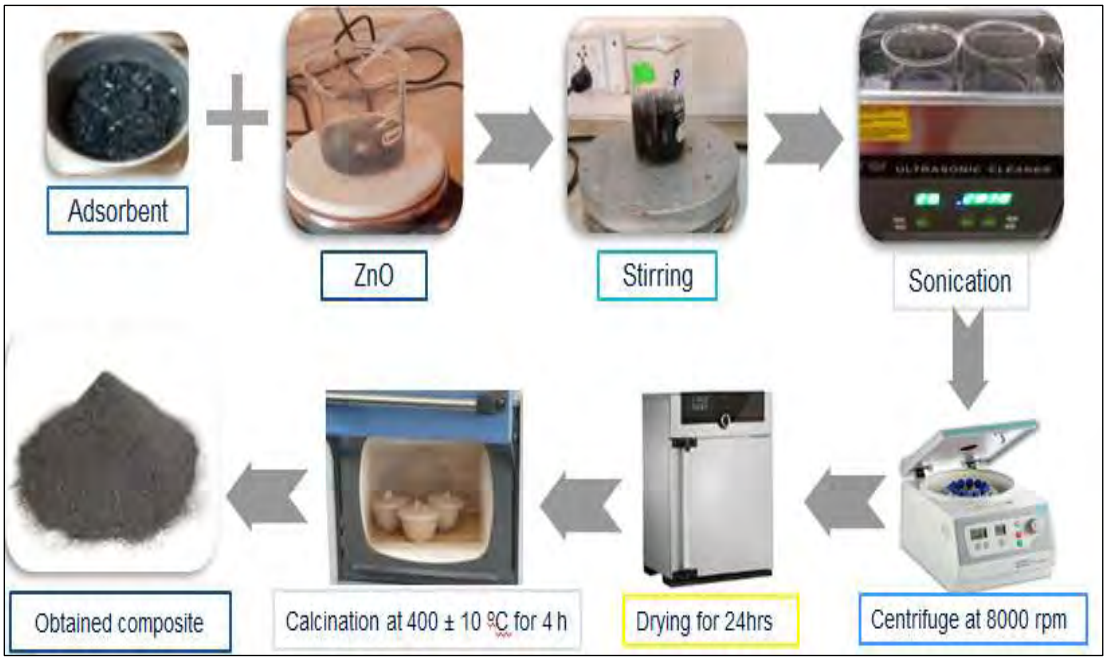

Figure 2.2 schematic representation of the composite

2.6 Degradation Efficiency

Levofloxacin and cadmium were used to test the catalyst's ability to promote degradation. Levofloxacin in a working volume of 50 ml and cadmium solution with a concentration of 10 mg per liter (each) were taken in two separate beakers and added, together with 10 mg of catalyst, for the process evaluation. In distilled water, the solutions were created. To assure the accomplishment of adsorption-desorption equilibrium, the solutions were agitated in the dark for 30 minutes prior to illumination. Using NaOH and HCl, the produced samples' pH was brought down to 7.0. The photocatalytic activity was investigated by exposing the experiment to sunshine for 180 minutes while continuously stirring after keeping the solutions in the dark. Same procedure was opted for the adsorption mechanism by keeping the solutions in dark on the orbital shaker at 160 rpm. The degradation of both the pollutants (%) was determined using the following equation:

$$\boldsymbol{Degradation\ Efficiency}\ \% = \left(\frac{C_0 - C}{C_0}\right) x\ 100 \qquad (2.1)$$

2.7 Characterization Techniques

2.7.1 Fourier-Transform Infrared Spectroscopy (FTIR)

FTIR is used to characterize the material by employing infrared light for identifying certain functional groups in the sample. When IR radiation strikes an object, some of it is absorbed by it and some of it flows right through it. [21]

A basic interferometer creates an optical signal that contains all of the infrared frequencies. The Fourier transformation, a mathematical technique, is then used for decoding the signal. The spectral data are then mapped using this computer-generated method.[22]

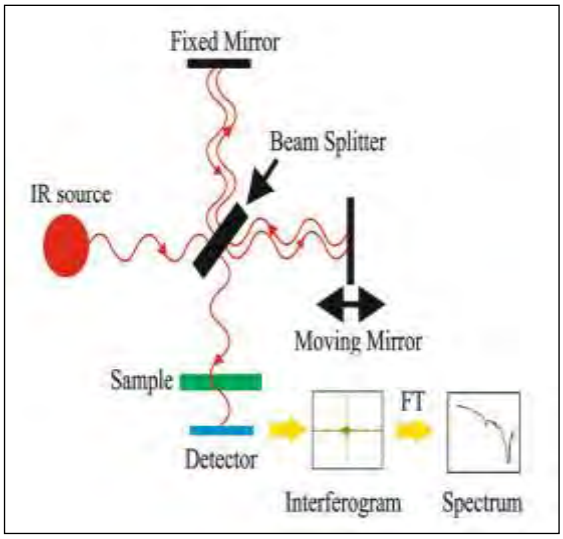

Figure 2.3 working of FTIR

2.7.2 X-Ray Diffraction (XRD)

XRD is regarded as a potent technique for characterizing crystalline structure. It tells us about the textures, structures, and orientations of crystals. Particle size, crystallinity, stresses, and flaws in crystal structures are some additional variables that can be studied using the XRD approach. X-rays are diffracted at particular angles when a monochromatic light beam strikes a material, creating XRD peaks. Peak intensities give information about the distribution of atoms and the lattice structures.[23] It consists of an X-ray source, radiation detector and signal processor. **(Figure 2.4).**

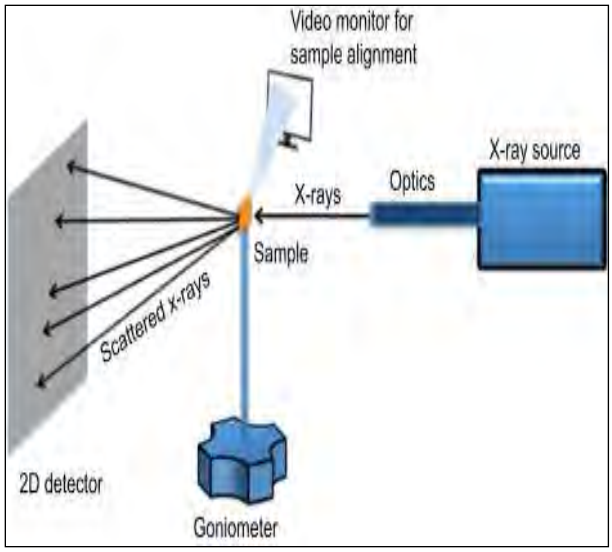

Figure 2.4 x-ray diffraction (XRD)

Bragg's law, which states that any 3D crystal lattice can be evaluated when constructive interference occurs between its crystal planes, which in turn gives the information on the d-spacing of crystal lattice of any crystalline or layered material, states that X-ray diffraction in a crystal will only occur if the conditions for that law are satisfied.

$$n\lambda = 2d\sin\theta \qquad (2.2)$$

Where, n is any integer displaying order of diffraction, λ is the wavelength of incident x-ray beam, d is for the spacing between crystal lattice planes and θ is Bragg's angle of diffraction from different planes [24]

2.7.3 Ultraviolet Visible Spectroscopy

The basis of spectroscopy is the interaction of light and matter. A spectrum is created when a substance absorbs light using excitation and de-excitation processes. When matter that contains electrons absorbs UV rays, excitation occurs. The effect is that they suddenly switch from their ground state, which has very little energy, to their excited state, which contains a lot of energy. Remember that the energy difference between an electron's ground state and excited state is always equal to the amount of ultraviolet or visible light the electron will absorb [25].

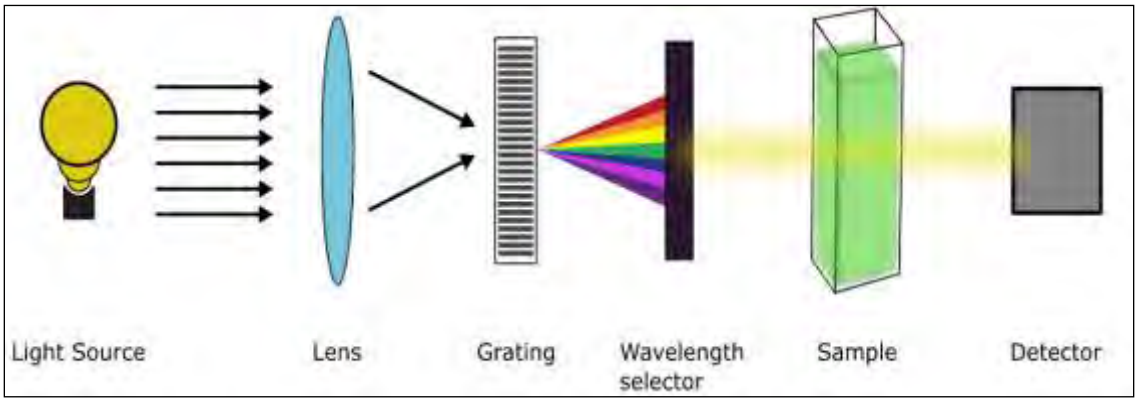

Figure 2.5 ultraviolet visible spectroscopy

The Beer-Lambert Law, which stipulates that there is a straight proportionality between absorbance and concentration, is the guiding principle behind absorbance spectroscopy. Depending on the concentration of the analyte present in the solution, light with a given

wavelength that strikes the analyte is either absorbed or transmitted .[26]

The **Equation 2.3** given below is the mathematical representation of Beer-Lambert law:

$$A = \varepsilon cl \qquad (2.3)$$

Where, A is absorbance of the catalyst, ε is the molar absorptivity constant that is different for every chemical at every wavelength, l is optical path length and c is concentration of the solution.

2.7.4 Scanning Electron Microscopy (SEM)

SEM, or scanning electron microscopy, uses an electron beam to magnify and create high resolution images of objects by scanning their surfaces. A fine stream of high-energy electrons impinging on a specimen's surface and the subsequent collecting of numerous signals from the specimen surface to ascertain its attributes form the basis of SEM technology. [27]

By using SEM, different images with various resolving power can be obtained. SEM is an efficient instrument with having high resolution, greater magnification, and large depth of field. It can scan the material that have size of approximately 1 cm to 5 micrometers and has spatial resolution up to 50 to 100 nm. Due its lager depth of field it can focus on large sample and produce three dimensional images of sample at a time.[28]

The instrument used for SEM includes the following components; an electron source, anode, condenser lens, scanning coils and the objective lens.

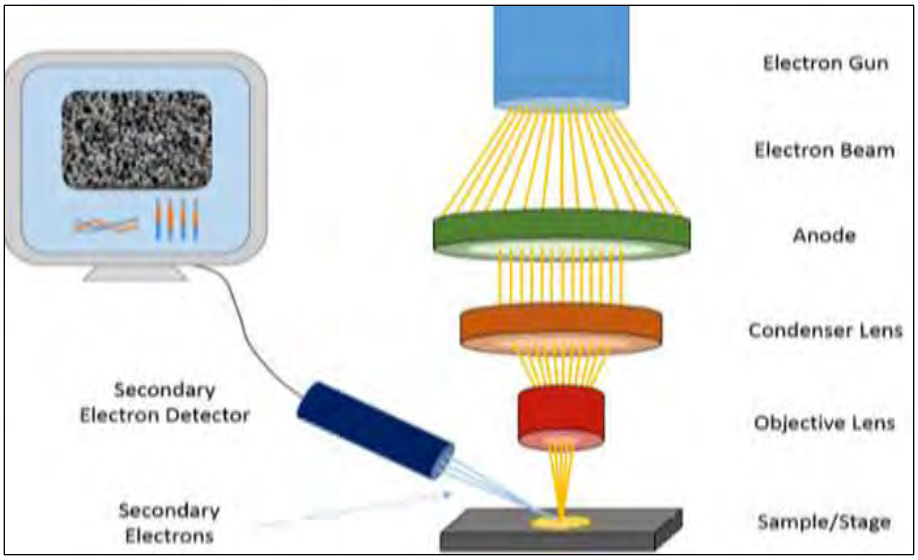

Figure 2.6 scanning electron microscopy (SEM)

2.7.5 Energy Dispersive X-Ray Spectroscopy (EDS)

Energy-dispersive X-ray spectroscopy, also known as EDS or EDX, is a potent method that enables the user to evaluate the elemental composition of a selected sample. The primary mechanism by which EDS operates is the ability of high intensity electromagnetic radiation (X-rays) to eject "core" electrons from an atom—electron that is not in the outermost shell.

The hole produced by the departure of these electrons can be filled by an electron with higher energy, and when it relaxes, it will release energy. By measuring the energy released during this relaxing process, which is unique to each element on the periodic table, one may identify which elements are present in a sample and in what amounts. [29] EDS functions with a series of three major parts; an emitter, a collector and an analyzer.

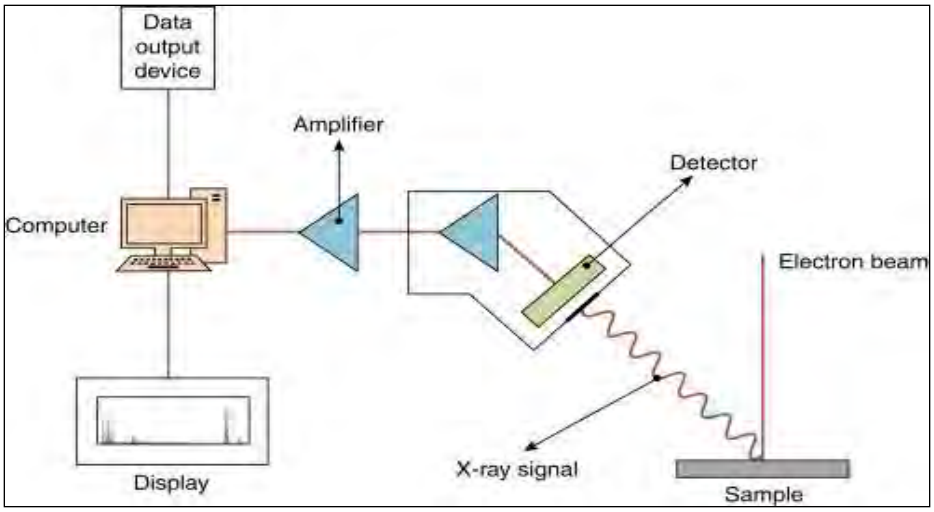

Figure 2.7 energy dispersive x-ray spectroscopy (EDS)

3. RESULTS

3.1 Ultraviolet Visible Spectroscopy

Instrument NIR spectrophotometer UV Vis 3600 plus was used to check the charge behavior and optical properties of the prepared photocatalyst i.e., Biochar-ZnO Composite. The band gap of prepared catalyst was estimated using Kubelka-Munk function as shown in the give equation

$$FR \times h\upsilon = B\,(h\upsilon - Eg) \qquad \textbf{(3.1)}$$

Where FR is Kubelka-Munk function, $h\upsilon$ is Energy of photon and its value can be calculated by 1240/λ. Eg is band gap of sample that can be calculated from above **Equation 3.1**. Peaks are obtained by plotting $(FR \times h\upsilon)^2$ on Y axis, and $h\upsilon$ on axis as shown in the **Figure 3.1**. It can be seen that the band gap of BC-ZnO composite is 2.9 eV. This indicates that the above sample has a desirable bandgap to degrade organic pollutants under visible light.

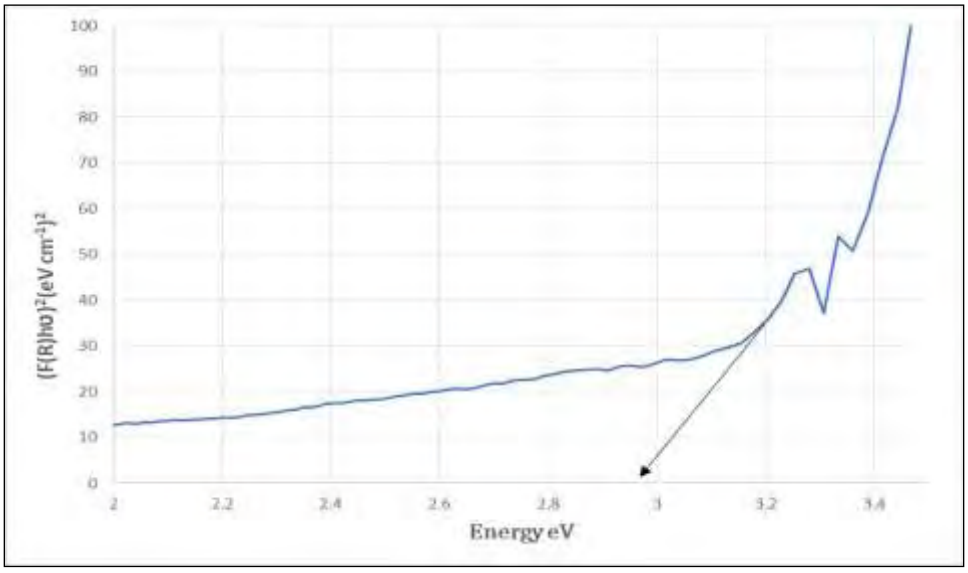

Figure 3.1 band gap determination through ultraviolet visible spectroscopy

3.2 X-Ray Diffraction (XRD)

The X-ray diffraction (XRD) patterns were recorded to determine the crystallinity of the materials. The diffraction peaks of 2θ were determined in the range of 20–70. **Figure 3.2** illustrates the diffraction patterns of pure ZnO, carbon, and their composite. The carbon peak on plane 002 indicates the crystalline structure of carbon derived from apricot shells, which provides the active sites for the adsorption of the pollutant. [30] In ZnO, major peak facets are (100), (101), (102), (110), (103) and (112). The composite spectra show suppressed ZnO peaks, indicating that ZnO particles were successfully embedded.

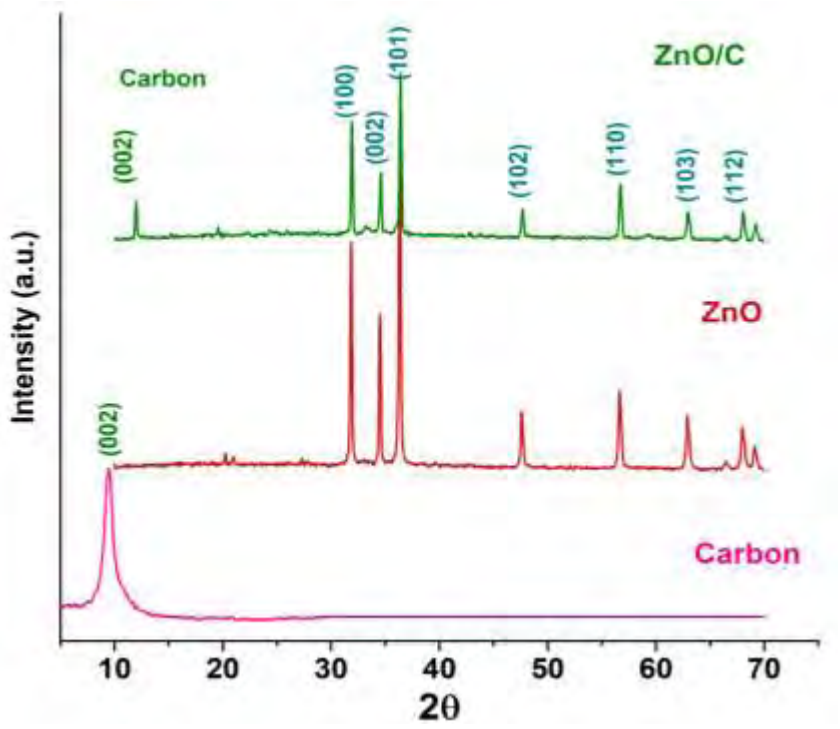

Figure 3.2 x-ray diffraction data of the catalyst

3.3 Fourier-Transform Infrared Spectroscopy (FTIR)

In order to evaluate the functional groups in the synthesized composite, Fourier transform infrared (FTIR) study was carried out. The FTIR results of prepared sample were determined in range of 400–4000 cm^{-1} wave number as shown in **Figure 3.3**. In the FTIR spectra of Carbon-ZnO composite, the sharp peak near 1700 cm^{-1} is ascribed to the structural vibration of benzene

ring. Two more sharp peaks between 1300–1100 cm^{-1} in the spectra, confirmed the presence of C-N stretching of aromatic amine.

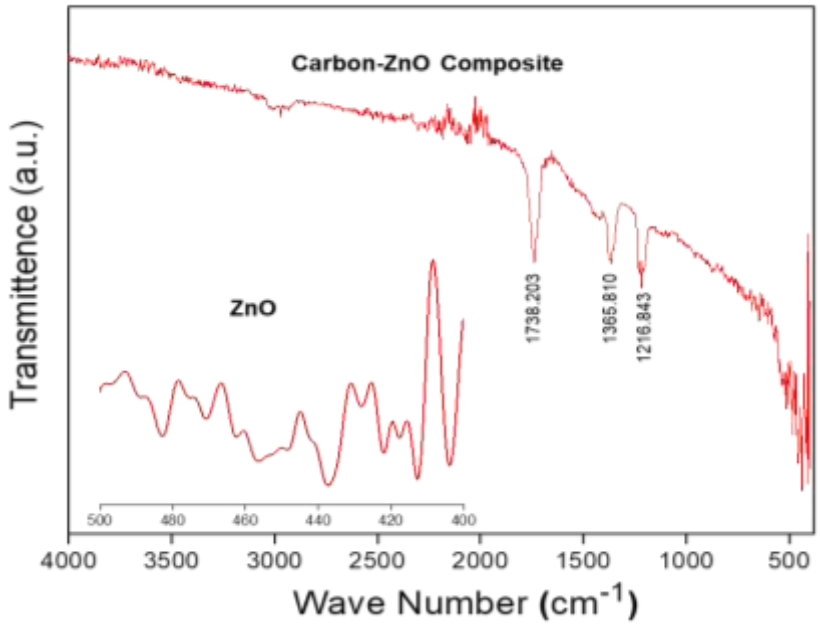

Figure 3.3 FTIR spectra in 0–4000 cm^{-1} range for C-ZnO composite

3.4 Scanning Electron Microscopy (SEM)

The structural morphology of the synthesized samples was examined using the SEM method. **Figure 3.4** displays the SEM images of carbon, ZnO, and their composite. The carbon sample consists of large clusters in **Figure 3.4(a)**, each of which has a smooth surface that serves as a loading edge for the addition of ZnO nanoparticles. The surface morphology of a pure ZnO sample is shown in **Figure 3.4(b)**, clearly displaying spherical aggregates of ZnO nanoparticles. The SEM pictures of the ZnO-impregnated carbon in **Figure 3.4(c)** revealed significant morphological changes; it appeared as though the pores on the surface of the carbon were occupied by ZnO, resulting in the creation of homogeneous coverage and the successful synthesis of composite photocatalyst.

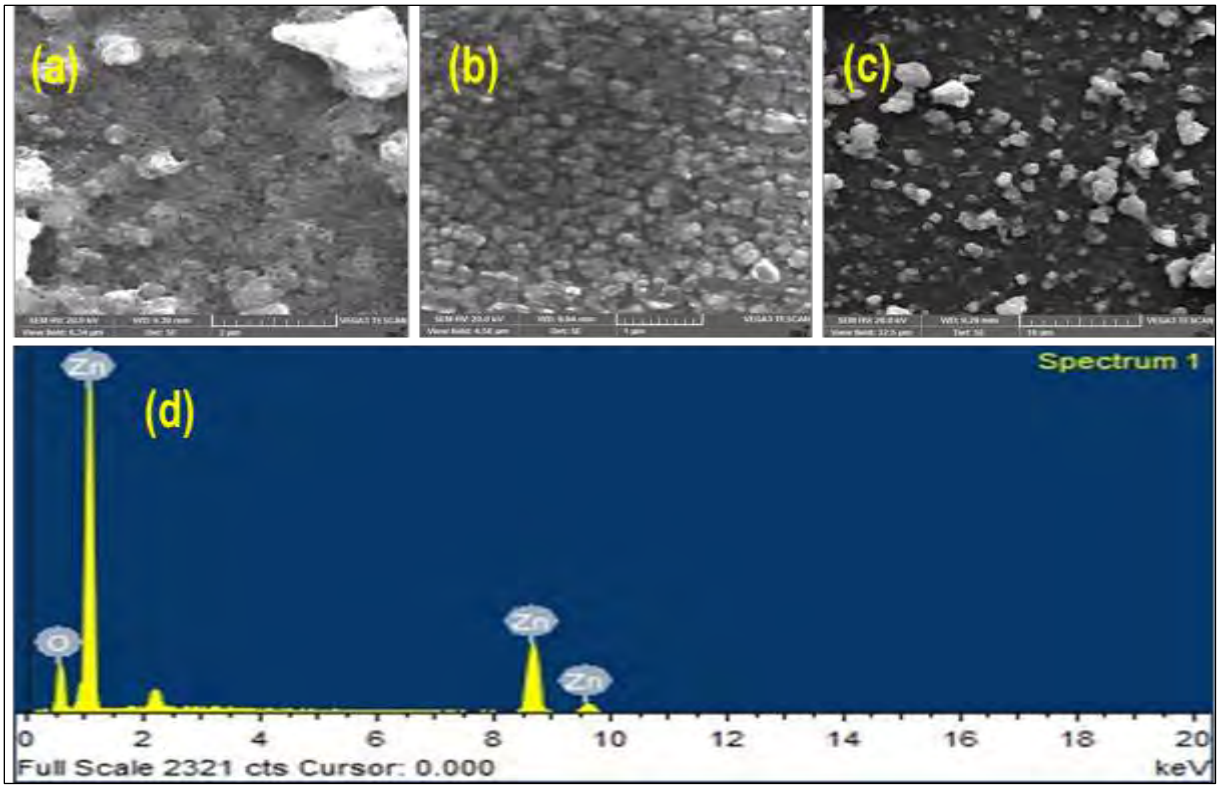

Figure 3.4 SEM images of **(a)** carbon **(b)** ZnO nanoparticles and **(c)** Carbon-ZnO composite **(d)** EDX analysis of ZnO

3.5 Energy Dispersive X-Ray Spectroscopy (EDS)

Elemental composition surveys are done using EDS. It also gives information about the weight percentage of elements present in the sample. According to **Table 3.1**, EDS of ZnO showed 71.77 zinc and 28.23 oxygen by weight percentage whereas 38.36 zinc and 61.64 oxygen by atomic percentage supporting the fact that the material is pure and uniformly formed without any additional element.

Figure 3.4 (d) shows the elemental composition of ZnO. Peaks of zinc (Zn) and oxygen (O) are clearly observed, that indicates the final composition of the sample is exclusively zinc and oxygen components.

Table 3.1 ZnO composition analysis using EDS

Element	App Conc.	Intensity Corrn.	Weight %	Atomic %
O K	18.15	0.6336	28.23	61.64
Zn K	66.42	0.9127	71.77	38.36

3.6 Evaluation of Photocatalytic Performance using Photocatalyst

Levofloxacin and cadmium were both tested for their photocatalytic degradation. All synthesized samples were evaluated in sun light at 120,000 lux. It was prepared with pure levofloxacin and cadmium acetate. Levofloxacin and cadmium solutions containing 10 ppm each were taken separately in two separate beakers for testing, along with 10 mg of catalyst.

To assure the accomplishment of adsorption-desorption equilibrium, the solutions were agitated in the dark for 30 minutes prior to illumination. After 180 minutes of exposure to sunlight with constant stirring, the experiment was subjected to the analysis of photocatalytic activity. Sample was collected after specific time intervals (0, 30, 60, 90, 120, 150 and 180 min) and separated using centrifuge at 5000 rpm for 5 minutes. After that absorption of levofloxacin and cadmium was measured by using UV-Visible spectrum. **Figure 3.5 a** and **b** shows absorbance spectra of levofloxacin and cadmium. A visual degradation can be seen with the passage of time.

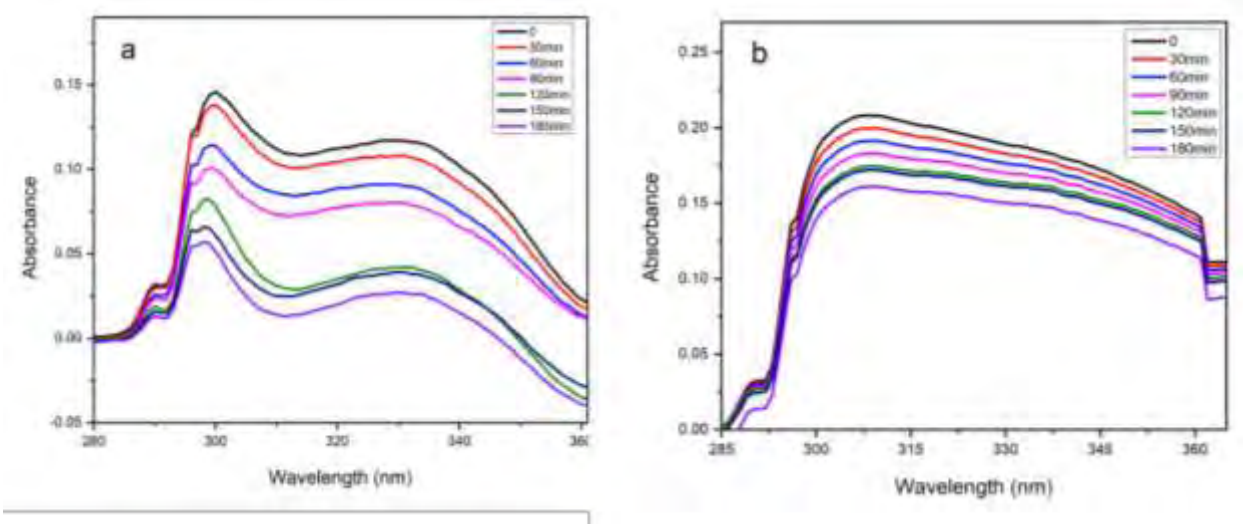

Figure 3.5 UV-vis absorbance spectra of **(a)** levofloxacin **(b)** cadmium using C-ZnO Composite

3.7 Effect of Photolysis

Before studying the effect of photocatalyst on the degradation of Cadmium and Levofloxacin, natural degradation was investigated. For that purpose both the pollutants solution was kept in solar light irradiation for 180 minutes. Negligible photolysis was observed in both the solutions in absence of any catalyst as shown in **Figure 3.6 (a)** and **(b)**.

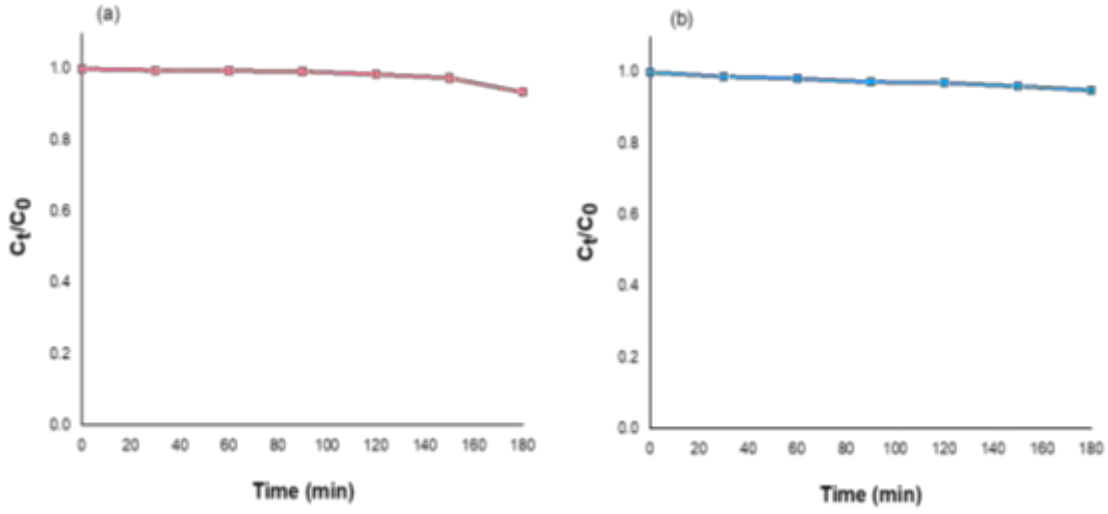

Figure 3.6 photolysis of **(a)** levofloxacin and **(b)** cadmium under solar light for 3 hours

3.8 Optimization Study

To study the effect of various independent parameters on the photocatalytic activity of the photocatalyst, following tests were performed; effect of catalyst dose, effect of pollutant concentration and effect of pH change.

3.8.1 Optimization Study of Levofloxacin

3.8.1.1 Effect of Catalyst Dose:

Different amount of catalyst concentrations has different effect on the rate of degradation. Reaction kinetics was checked by 3 different doses of catalyst i.e. 10 mg/L, 20 mg/L and 30 mg/L. Simultaneous adsorptive and photocatalytic experiments were carried out at different doses of catalyst while the concentration of levofloxacin was kept constant for each experiment. **Figure 3.7** shows that as a result of the adsorption activity, highest percentage adsorption was carried out by 30mg/L dose of the catalyst i.e. 65.7%, 64% by 20mg/L and 42% by 10mg/L respectively. Whereas **Figure 3.8** shows **(a)** photocatalytic degradation of levofloxacin and **(b)** its respective natural log of C_t/C_0 graph in which 30mg/L of the catalyst resulted in highest degradation followed by 20mg/L and 10mg/L respectively.

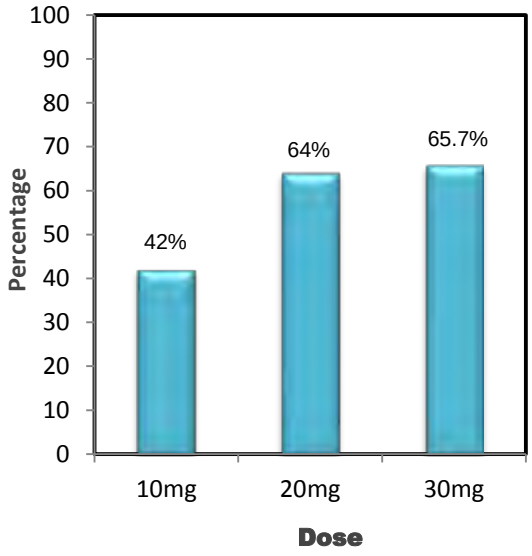

Figure 3.7 percentage adsorption of levofloxacin on three different catalyst doses

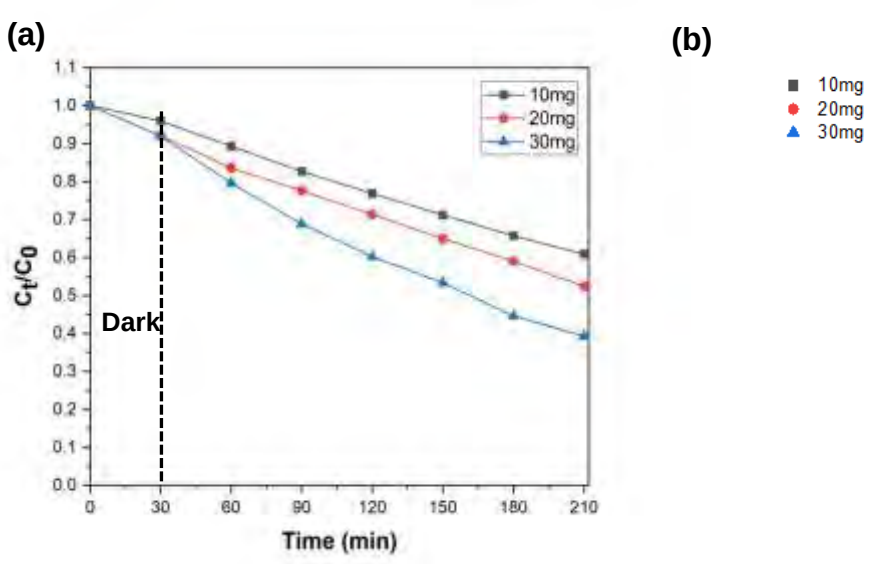

Figure 3.8 (a) effect of different doses of catalyst on the photocatalytic degradation of levofloxacin **(b)** $\ln C_t/C_o$ versus time plot.

3.8.1.2 Effect of Pollutant Concentration

The effect of pollutant concentration on reaction kinetics was checked at four different concentrations of levofloxacin but at constant catalyst dose of 30 mg/L. According to **Figure 3.9**, highest percentage adsorption rate was observed in 5ppm solution i.e. 65.7%, 54% in 10ppm, 20% in 20ppm whereas 14.8% in 30ppm solution. While highest photocatalytic degradation was carried out in 10ppm solution followed by 5, 20 and 30 ppm respectively **(Figure 3.10).**

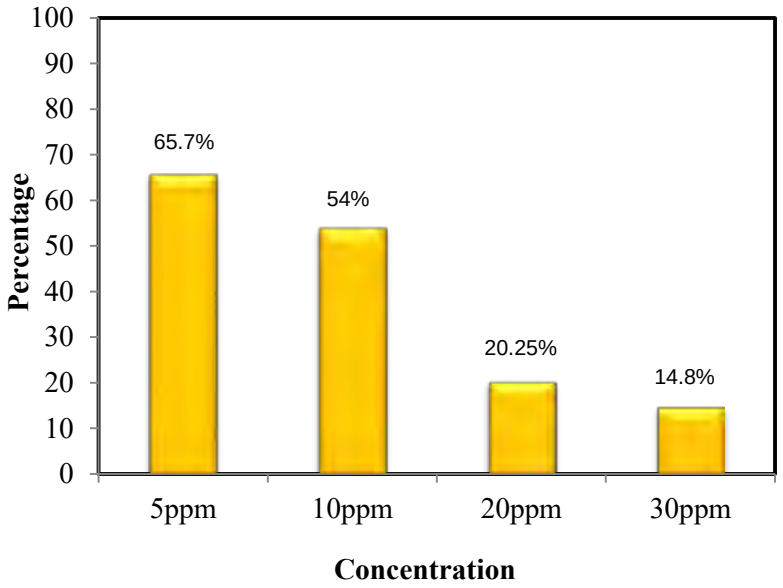

Figure 3.9 effect of four different pollutant concentrations on adsorption of levofloxacin

Figure 3.10 (a) effect of different pollutant concentrations on the photocatalytic degradation of levofloxacin **(b)** $\ln Ct/C_o$ versus time plot.

3.8.1.3 Effect of pH Change

Effect of different pH values (5, 7 and 9) was checked to calculate the efficiency of the catalyst to degrade levofloxacin. 1M HNO_3 and NaOH solutions were added to initial solution to adjust the pH. **Figure 3.11** shows that the highest degradation occurs at pH 5 (27%) followed by pH 7 (21%) and pH 9 (18%) respectively. Similarly in **Figure 3.12 (a)** highest photocatalytic

degradation was observed at pH 5 followed by pH 7 while lowest degradation was observed at pH 9.

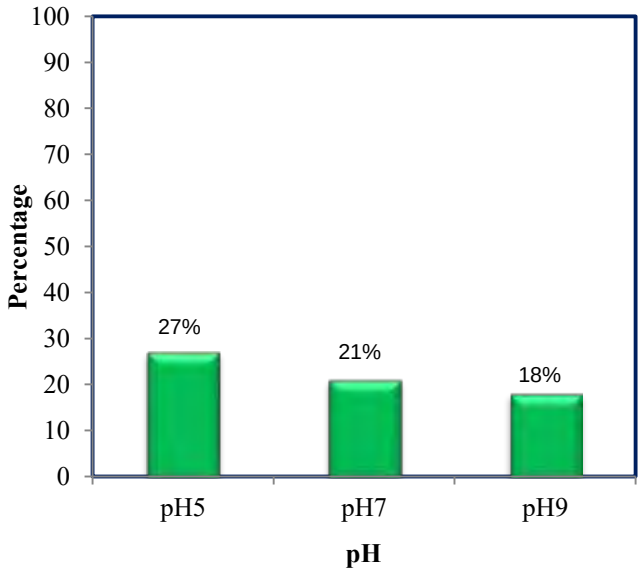

Figure 3.11 effect of pH change on the adsorption of levofloxacin

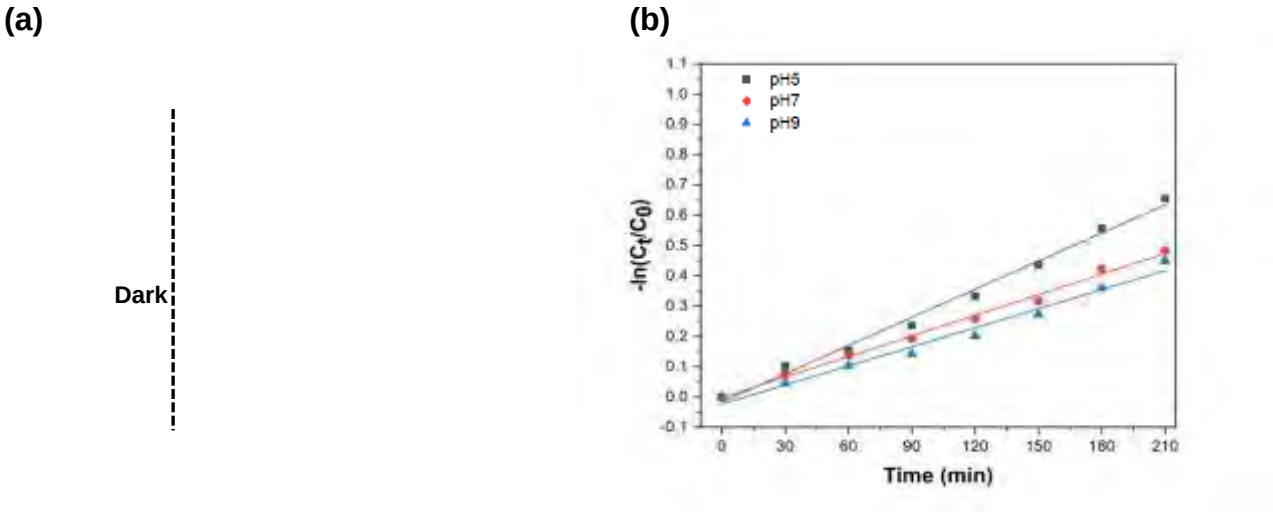

Figure 3.12 (a) effect of pH change on the photocatalytic degradation of levofloxacin **(b)** $\ln C_t/C_0$ versus time plot

3.8.1.4 Kinetics of Optimization Reactions of Levofloxacin

The results of all the optimization studies including adjacent R^2, rate constant values and percentage degradation are summarized in **Table 3.2**.

Table 3.2 overall reaction kinetics of levofloxacin

Experiment	Conditions	K min^{-1}	R^2	Percentage Degradation (%)
Effect of catalyst dose (mg/L)	10	$0.00243\pm6.11\times10^{-5}$	0.990057	39
	20	$0.00301\pm7.07\times10^{-5}$	0.99623	47.5
	30	**$0.00456\pm1.09\times10^{-4}$**	**0.99601**	**61**
Effect of levofloxacin concentration (ppm)	5	$0.00456\pm1.09\times10^{-4}$	0.99601	61
	10	**$0.00567\pm2.91\times10^{-4}$**	**0.98185**	**68**
	20	$0.0018\pm4.33\times10^{-5}$	0.99597	32.5
	30	$0.00136\pm9.31\times10^{-5}$	0.96804	27
Effect of pH	**5**	**$0.0031\pm1.20\times10^{-4}$**	**0.98948**	**48**
	7	$0.00226\pm7.24\times10^{-5}$	0.99287	38.25
	9	$0.0021\pm1.19\times10^{-4}$	0.977784	36

3.8.2 Optimization Study of Cadmium

3.8.2.1 Effect of Catalyst Dose

The effect of catalyst amount on reaction kinetics was checked at 3 different concentrations i.e., 10 mg, 20 mg and 30 mg while the concentration of cadmium was kept constant for each experiment. Simultaneous adsorptive and photocatalytic experiments were carried out at different doses of catalyst. **Figure 3.13** shows that at 30 mg catalyst dose, the adsorption is highest i.e. 31%, followed by 27.5% at 20 mg and 23% at 10 mg. Similarly in **Figure 3.14 (a)**

30mg/L of the catalyst resulted in highest photocatalytic reduction followed by 20mg/L and 10mg/L respectively.

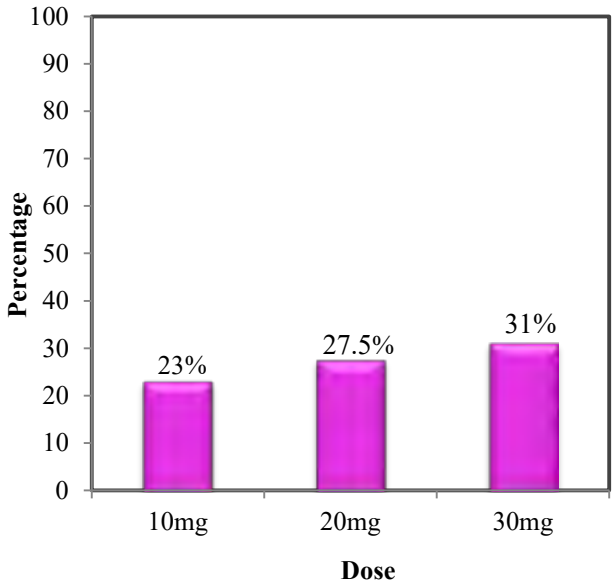

Figure 3.13 percentage adsorption of cadmium on three different catalyst dose

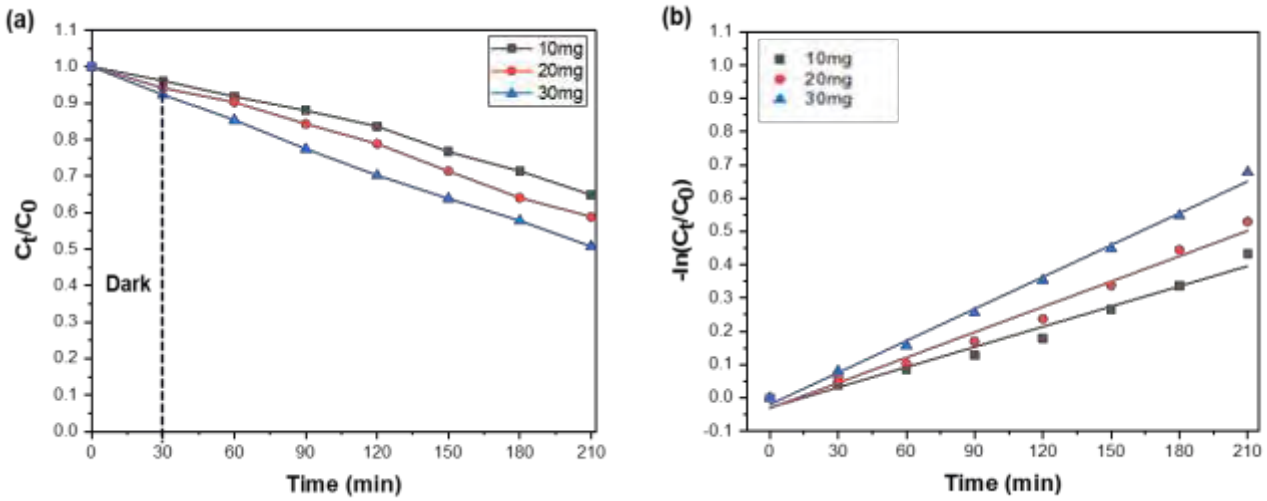

Figure 3.14 (a) effect of three different catalyst dose on the photocatalytic reduction of cadmium **(b)** $\ln Ct/C_o$ versus time plot

3.8.2.2 Effect of Pollutant Concentration

To evaluate the effect of pollutant concentration, experiments were conducted at four different concentrations of cadmium at constant catalyst dose of 30 mg. It is evident in the **Figure 3.15** that highest adsorption rate was observed in 10 ppm pollutant concentration i.e. 42%, 38% in 20 ppm, 35% in 10 ppm while the lowest rate was exhibited by 5 ppm solution which is 31%. According to **Figure 3.16 (a)**, the photocatalytic reduction was highest in 10 ppm followed by 5 ppm, 20 ppm and 30 ppm respectively.

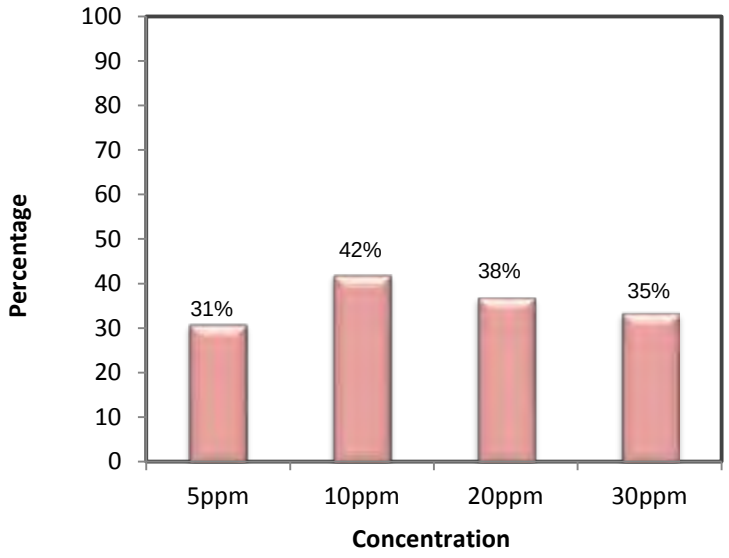

Figure 3.15 effect of four different pollutant concentrations on cadmium adsorption

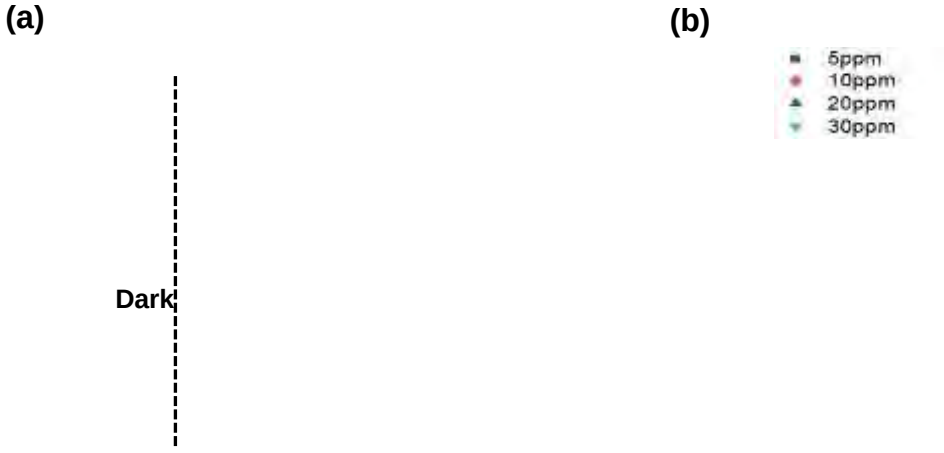

Figure 3.16 (a) effect of different pollutant concentrations on the adsorption of cadmium **(b)** $\ln C_t/C_o$ versus time plot.

3.8.2.3 Effect of pH Change

Effect of different pH values (5, 7 and 9) was checked to calculate the efficiency of the catalyst to reduce cadmium. 1M HNO_3 and NaOH solutions were added to initial solution to adjust the pH. **Figure 3.17** shows that cadmium was adsorbed comparatively more in acidic pH (45% at pH 5) than neutral (29% at pH 7) and basic (20% at pH 9) respectively. Similarly in **Figure 3.18 (a)** highest photocatalytic reduction was observed at pH 5, followed by pH 7 while lowest at pH 9.

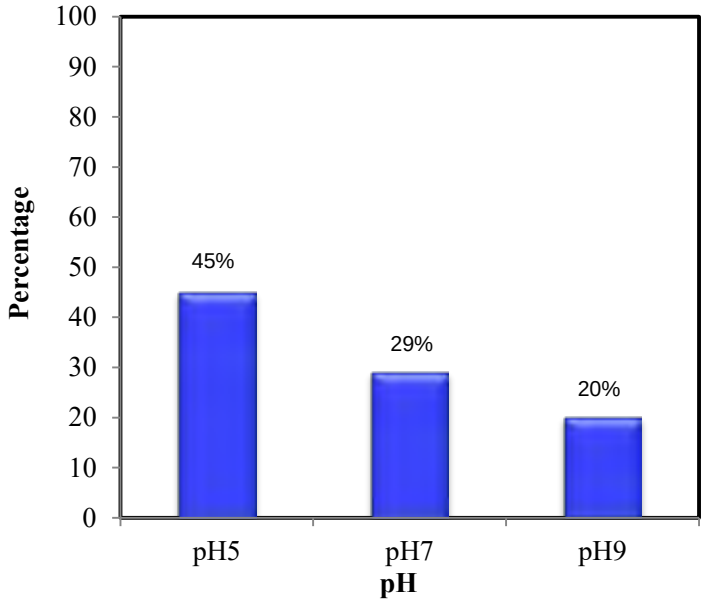

Figure 3.17 effect of pH change on cadmium adsorption

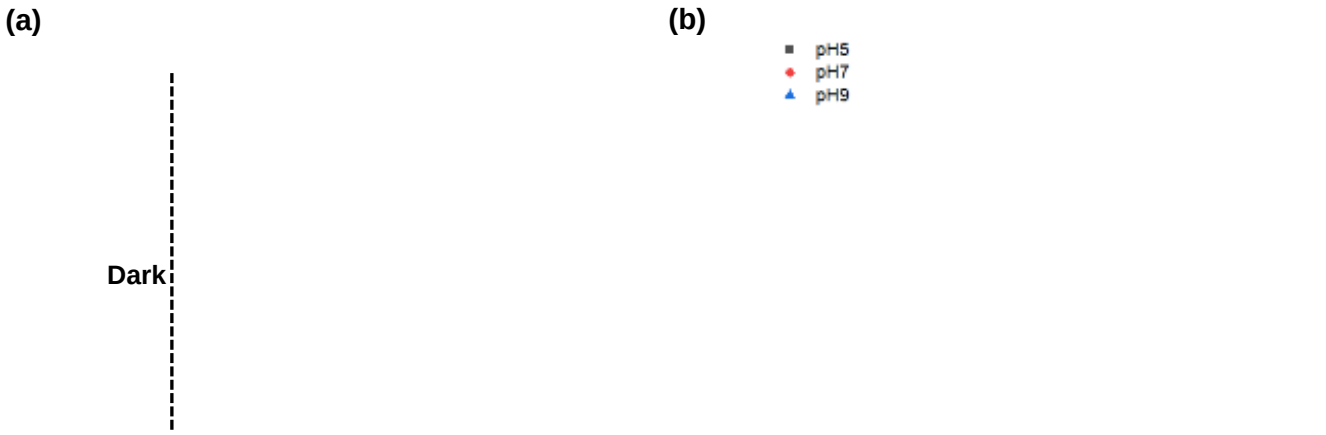

Figure 3.18 (a) effect of pH change on the photocatalytic reduction of cadmium **(b)** $lnCt/C_o$ versus time plot.

3.8.2.4 Kinetics of Optimization Reactions of Cadmium

The results of all the optimization studies including adjacent R^2, rate constant values and percentage reduction are summarized in **Table 3.3**.

Table 3.3 overall reaction kinetics of cadmium

Experiment	Conditions	K min^{-1}	R^2	Percentage Reduction (%)
Effect of catalyst dose (mg/L)	10	$0.00203\pm1.37x10^{-5}$	0.9687	35
	20	$0.00254\pm1.48x10^{-5}$	0.9771	41
	30	$\mathbf{0.0032\pm1.80x10^{-4}}$	**0.9946**	**49**
Effect of cadmium concentration (ppm)	5	$0.0032\pm4.80x10^{-5}$	0.9946	49
	10	$\mathbf{0.0039\pm1.05x10^{-4}}$	**0.9949**	**56**
	20	$0.00242\pm1.07x10^{-4}$	0.9862	40.7
	30	$0.00199\pm1.72x10^{-4}$	0.9496	33
Effect of pH	**5**	$\mathbf{0.00208\pm2.80x10^{-5}}$	**0.9987**	**35**
	7	$0.00133\pm5.63x10^{-5}$	0.9876	24.5
	9	$0.00108\pm3.32x10^{-5}$	0.9901	21

3.9 Adsorption Isotherms

Adsorption isotherm is fundamentally essential to describe how solutes interact with adsorbents. The influence of pollutant concentration on adsorption capacity was investigated using the following concentrations such as 5, 10, 20 and 30 ppm. According to **Figure 3.7** (levofloxacin adsorption) and **Figure 3.13** (cadmium adsorption), it can be seen that the adsorption (%) is decreased with the increase in pollutant concentration.

In this study, the isotherm models such as Langmuir, Freundlich, Temkin and Dubinin Radushkevich are employed to analyze the mechanism of levofloxacin and cadmium adsorption. The following **Equations (3.2)** to **(3.5)** express the above mentioned isotherm models:

Langmuir model: $$q_e = \frac{q_m K_L C_e}{1+K_L C_e} \quad \textbf{(3.2)}$$

Freundlich model: $$q_e = K_F C_e^{1/n} \quad \textbf{(3.3)}$$

Temkin model: $$q_e = \frac{RT}{b} ln(AC_e) \quad \textbf{(3.4)}$$

DR model: $$q_e = q_{D-R} e^{-K_{D-R}\varepsilon^2} \quad \textbf{(3.5)}$$

where, the maximum adsorption capacity and the pollutant concentration at equilibrium are presented as qmax and Ce, respectively. The rate constant of Langmuir and Freundlich models are denoted by K_L and K_F, respectively. The four models were plotted using non-linear fitting given below in **Figure 3.19 and 3.20**.

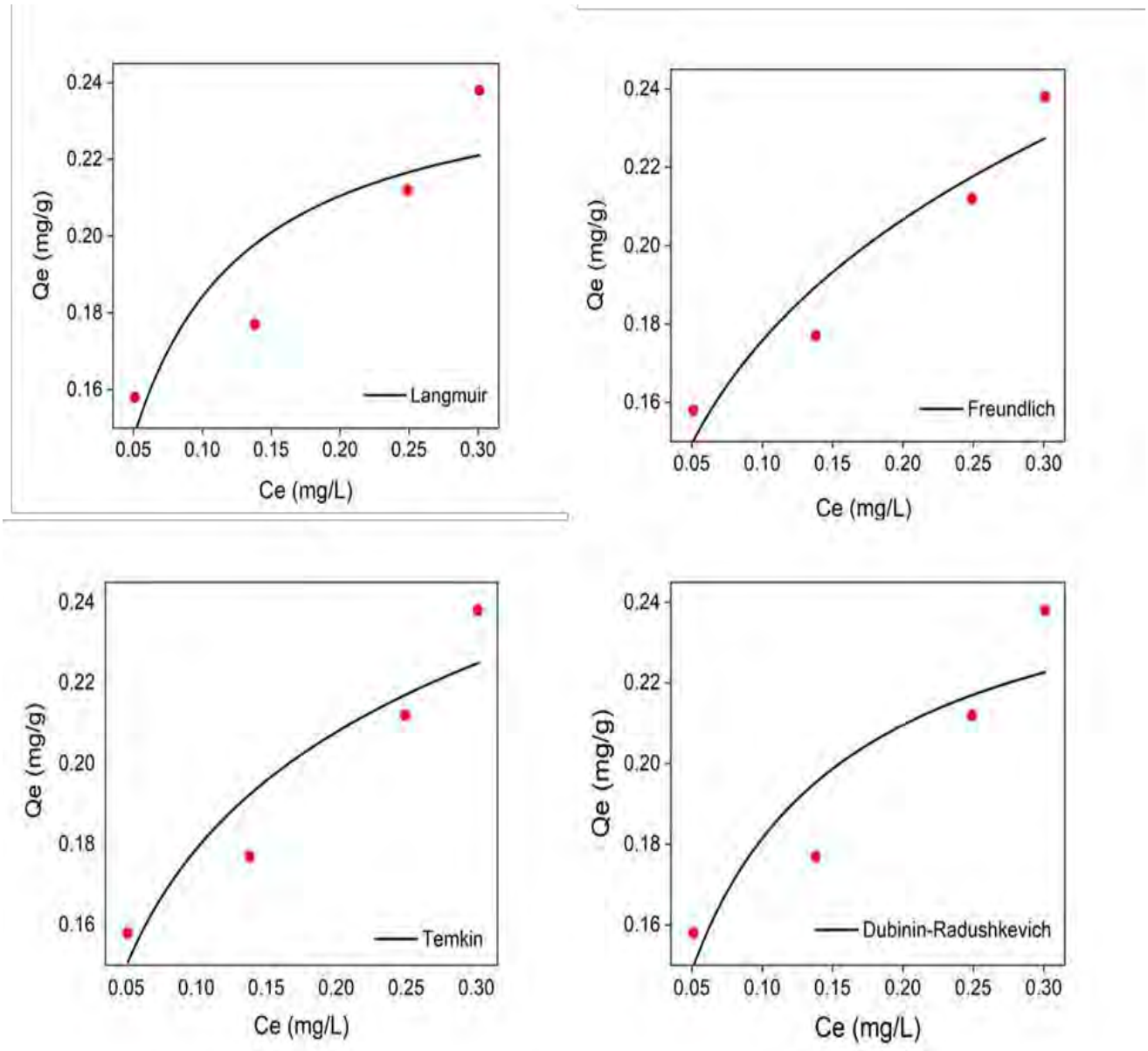

Figure 3.19 adsorption isotherm graphs of levofloxacin

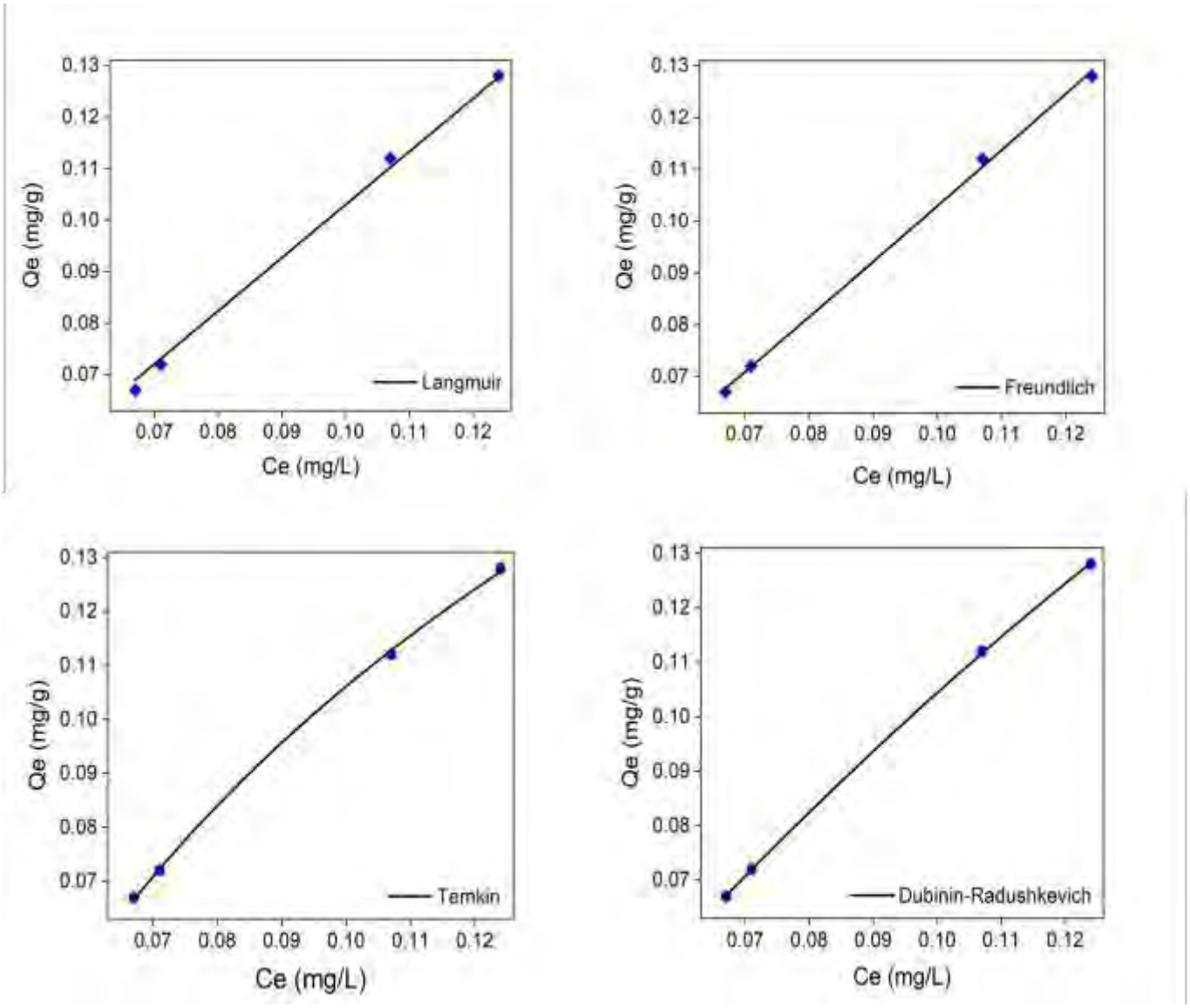

Figure 3.20 adsorption isotherm graphs of cadmium

The values of all four isotherm parameters are enlisted in the following **Table 3.4** on the basis of which the adsorption pathway was determined.

Table 3.4 isotherm models parameters

	Langmuir			**Freundlich**			**Temkin**			**D-R**		
	R^2	Q_{max} (mg g^{-1})	K_L	R^2	n	K_F (mg g^{-1})	R^2	B ($Jmol^{-1}$)	A (L mg^{-1})	R^2	Q_D (mg g^{-1})	E (kJ g^{-1})
Levo	0.67	0.245	30.11	**0.86**	0.234	0.30	0.81	0.418	722	0.74	0.251	0.057
Cd.	0.97	247.51	0.004	0.89	1.048	1.150	0.92	0.099	29.27	**0.99**	0.394	0.231

According to the R^2 values, it can be concluded that the favorable adsorption is carried out due to the multilayer diffusion of levofloxacin on to the heterogeneous surface sites of adsorbents. Therefore, for levofloxacin the most accurate isotherm is Freundlich (R^2 = 0.86) which shows that the adsorption is physical and multi-layered while Dubinin Radushkevich model is best fitted with experimental data of cadmium (R^2 = 0.99) indicating physical adsorption at micropores level..

3.10 Photocatalysis Mechanism Reaction

To investigate the reactive species responsible for the degradation of levofloxacin and reduction of cadmium, different scavenger tests have been performed with iso-propanol, EDTA, ascorbic acid and potassium dichromate for hydroxyl radical, hole, superoxide radical and electron respectively. To perform this experiment, a mixture of 50 mL of 10 ppm pollutant (cadmium as well as levofloxacin), 30 mg of catalyst and scavenging solution was exposed to visible light under stirring condition for 3 hours.

Figure 3.21 (a) shows the species involved in the levofloxacin degradation reaction; it can be found that by using ascorbic acid as trapping agent the photocatalytic reaction decreases drastically which shows that superoxide radical plays an important role in the photodegradation of the pharmaceutical levofloxacin. **Figure 3.21 (b)** shows the species involved in the cadmium reduction reaction in which ascorbic acid as well as potassium dichromate play a major role. Whereas by using iso-propanol and EDTA as the scavengers, the photocatalytic activity almost remains close to that of photocatalyst (without scavenger).

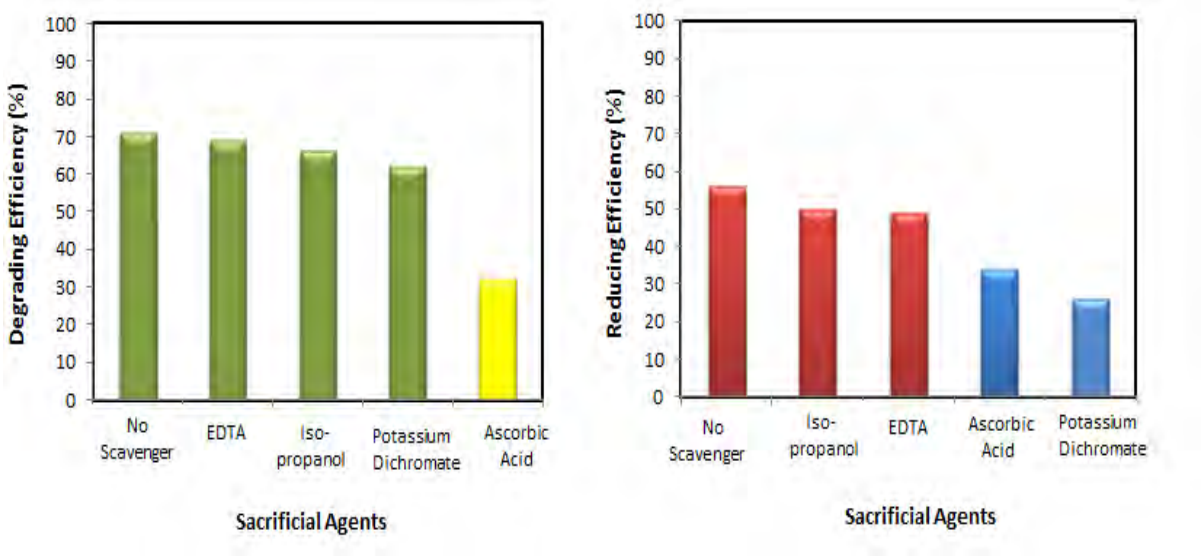

Figure 3.21 photocatalysis mechanism reaction of **(a)** levofloxacin **(b)** cadmium using four sacrificial agents

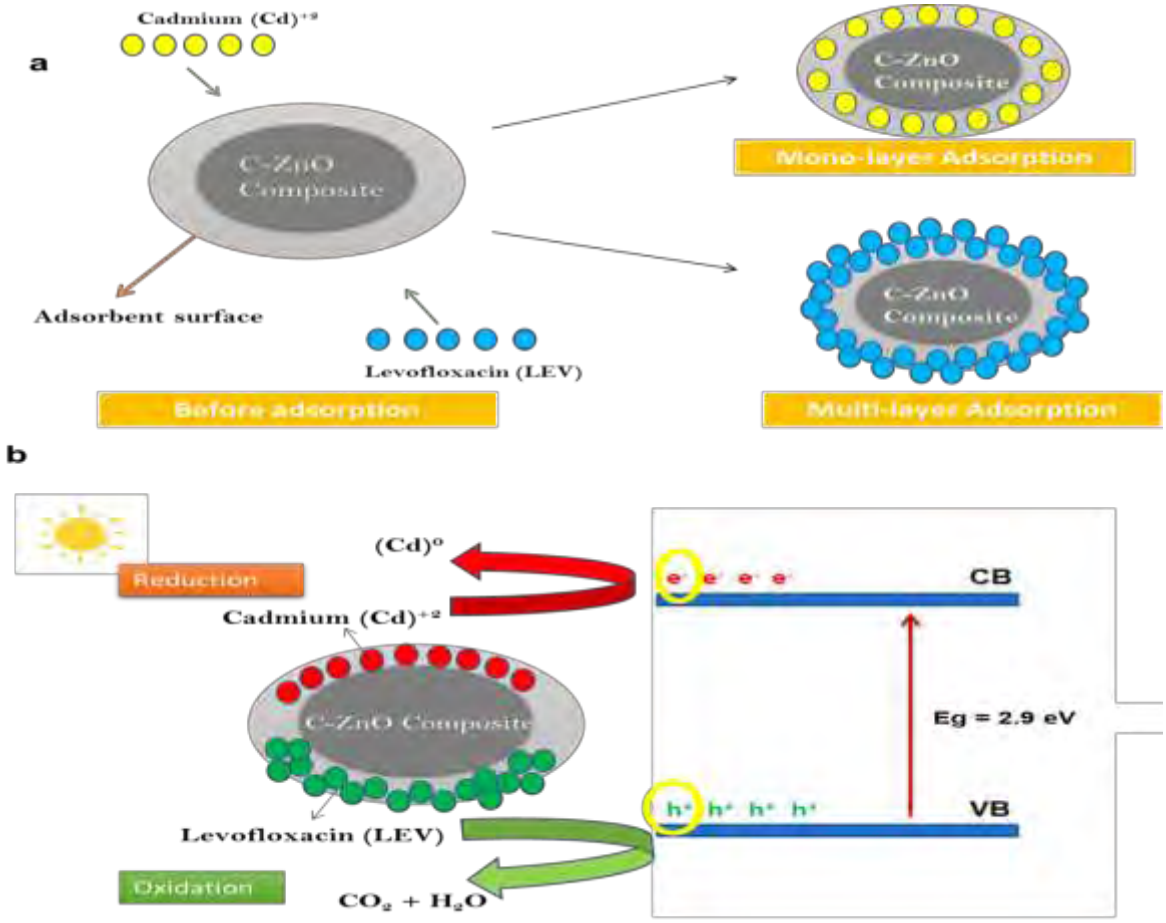

Figure 3.22 proposed scheme of (a) adsorption and (b) photocatalysis

4. CONCLUSION

In the present study, biomass derived carbon and ZnO composite was successfully synthesized by impregnating ZnO with carbon content. The nanoparticles of pure ZnO photocatalyst were prepared using the wet precipitation method. Results suggested that the prepared composite is very effective and stable adsorbent as well as photocatalyst for the degradation of levofloxacin and cadmium. It was able to degrade 56% cadmium and 68% levofloxacin. Therefore, this economical and sustainable composite can be utilized for the disintegration of pollutants from wastewater into less harmful compounds.

5. REFERENCES

1. S. F. Ahmed, M. Mofijur, S. Nuzhat, A. T. Chowdhury, N. Rafa, Md. A. Uddin, A. Inayat, T. M. I. Mahlia, H. C. Ong, W. Y. Chia and P. L. Show, Journal of Hazardous Materials, 2021, **416**, 125912.

2. UN World Water Development Report 2017, https://www.unwater.org/ publications/un-world-water-development-report-2017

3. H. C. Yap, Y. L. Pang, S. Lim, A. Z. Abdullah, H. C. Ong and C.-H. Wu, International Journal of Environmental Science and Technology, 2018, **16**, 601–628.

4. G. Lofrano, G. Libralato, R. Adinolfi, A. Siciliano, P. Iannece, M. Guida, M. Giugni, A. Volpi Ghirardini and M. Carotenuto, Ecotoxicology and Environmental Safety, 2016, **123**, 65–71.

5. A. Küster and N. Adler, Philosophical Transactions of the Royal Society B: Biological Sciences, 2014, **369**, 20130587.

6. Z. Li, Z. Ma, T. J. van der Kuijp, Z. Yuan and L. Huang, Science of The Total Environment, 2014, **468–469**, 843–853.

7. C. Ding, J. Chen, F. Zhu, L. Chai, Z. Lin, K. Zhang and Y. Shi, Frontiers in Environmental Science, 2022, **10**.

8. E. N. Zare, A. Motahari and M. Sillanpää, Environmental Research, 2018, **162**, 173–195.

9. Letters in Applied NanoBioScience, 2020, **10**, 2148–2166.

10. W. H. Hallenbeck, Cadmium in the Environment, 1986, 131–137.

11. Cadmium sources and toxicity, 2019.

12. G. Genchi, M. S. Sinicropi, G. Lauria, A. Carocci and A. Catalano, International Journal of Environmental Research and Public Health, 2020, **17**, 3782.

13. D. Yang, J. Li, L. Luo, R. Deng, Q. He and Y. Chen, Chemical Engineering Journal, 2020, **387**, 124103.

14. L. Saya, V. Malik, D. Gautam, G. Gambhir, Balendra, W. R. Singh and S. Hooda, Science of The Total Environment, 2022, **813**, 152529.

15. R. Rashid, I. Shafiq, P. Akhter, M. J. Iqbal and M. Hussain, Environmental Science and Pollution Research, 2021, **28**, 9050–9066.

16. S.-H. Lin and R.-S. Juang, Journal of Environmental Management, 2009, **90**, 1336–1349.

17. M. A. Rauf and S. S. Ashraf, Chemical Engineering Journal, 2009, **151**, 10–18.

18. M. M. Mian and G. Liu, RSC Advances, 2018, **8**, 14237–14248.

19. Mankomal and H. Kaur, Applied Surface Science Advances, 2022, **12**, 100339.

20. M. Amir, T. Fazal, J. Iqbal, A. A. Din, A. Ahmed, A. Ali, A. Razzaq, Z. Ali, M. S. Rehman and Y.-K. Park, Journal of Industrial and Engineering Chemistry, 2022, **115**, 171–182.

21. J. Mathias, Innovatech Labs, 2023.

22. Z. Movasaghi, S. Rehman and Dr. I. ur Rehman, Applied Spectroscopy Reviews, 2008, **43**, 134–179.

23. H. Khan, A. S. Yerramilli, A. D'Oliveira, T. L. Alford, D. C. Boffito and G. S. Patience, The Canadian Journal of Chemical Engineering, 2020, **98**, 1255–1266.

24. M. A. Thakar, S. Saurabh Jha, K. Phasinam, R. Manne, Y. Qureshi and V. V. Hari Babu, Materials Today: Proceedings, 2022, **51**, 319–324.

25. M. Darbandi, UV-VIS and Photoluminescence Spectroscopy for Nanomaterials Characterization, 2013, 431–452.

26. A. Das, Portable Spectroscopy and Spectrometry, 2021, 179–207.

27. J. W. Gooch, Encyclopedic Dictionary of Polymers, 2011, 922–922.

28. G.-W. Lee, J. Hee Kwon, S.-C. Jang, C. Roh, K. Myung and Y. Suk Huh, Microscopy and Microanalysis, 2017, **23**, 1384–1385.

29. D. Shindo and T. Oikawa, Analytical Electron Microscopy for Materials Science, 2002, 81–102.

30. C. Hu, X. Hu, R. Li and Y. Xing, Journal of Hazardous Materials, 2020, **385**, 121599.